Active force generation contributes to the complexity of spontaneous activity and to the response to stretch of murine cardiomyocyte cultures

Seyma Nayir[1], Stéphanie P. Lacour[2] and Jan P. Kucera[1]

[1] Department of Physiology, University of Bern, Bern, Switzerland

[2] Laboratory for Soft Bioelectronic Interfaces, EPFL, Geneva, Switzerland

Running title:

Active force, stretch and cardiac pacemaker activity

Keywords:

mechano-electric feedback, pacemaker function, heart rate variability, beat rate variability, stretch-activated channels, cardiac cell cultures, stretchable microelectrode arrays, blebbistatin, streptomycin

Table of Contents Category: Cardiovascular

Corresponding author:

Jan P. Kucera

Department of Physiology, University of Bern, Bühlplatz 5, CH-3012 Bern, Switzerland

E-mail: jan.kucera@unibe.ch

Key points summary

- Monolayer cultures of cardiac cells exhibit spontaneous electrical and contractile activity, as in a natural cardiac pacemaker. Beating variability in these preparations recapitulates the power-law

This is an Accepted Article that has been peer-reviewed and approved for publication in The Journal of Physiology, but has yet to undergo copy-editing and proof correction. Please cite this article as an 'Accepted Article'; doi: 10.1113/JP283083.

behavior of heart rate variability in vivo. However, the effects of mechano-electrical feedback on beating variability are not yet fully understood.

- Using stretchable microelectrode arrays, we examined the effects of the contraction uncoupler blebbistatin and the non-specific stretch activated channel blocker streptomycin on beating variability and on stretch-induced changes of beat rate.
- Without stretch, blebbistatin decreased the spatial complexity of beating variability, while streptomycin had no effects.
- Both stretch and release transiently increased beat rate; blebbistatin attenuated the increase of beat rate upon stretch, while streptomycin had no effects.
- Active force generation contributes to the complexity of spatiotemporal patterns of beating variability and to the increase of beat rate upon mechanical deformation. Our study contributes to understanding how mechano-electric feedback influences heart rate variability.

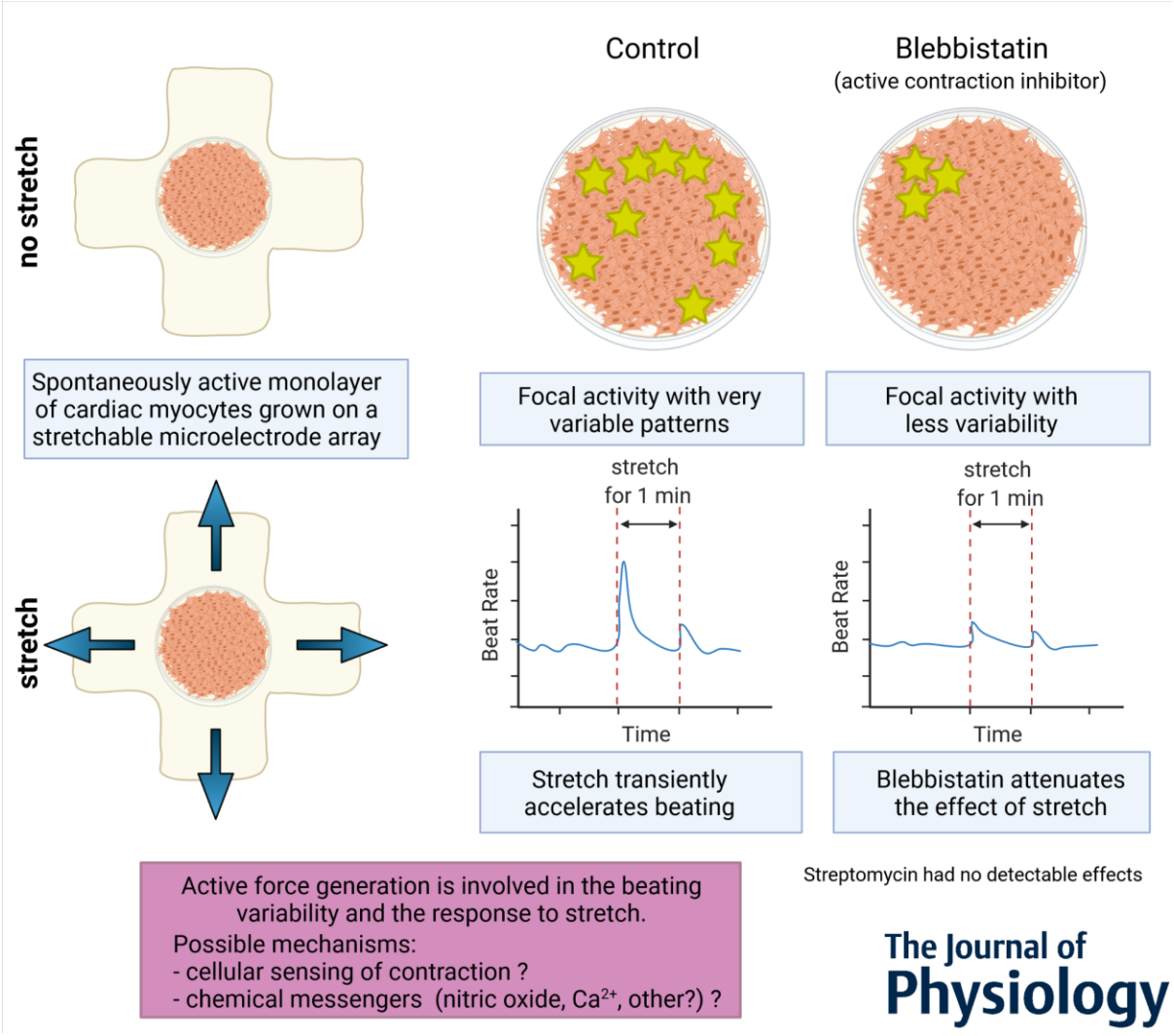

Abstract Figure Legend

Mechano-electric feedback modulates myocardial electrical function, including pacemaking. By growing monolayer cultures of spontaneously active murine cardiac cells on stretchable microelectrode arrays, we examined whether active contractions influence the spatiotemporal characteristics of beating variability and the effects of stretching on beat rate. Under control conditions (no stretch and no pharmacological agent), the origin of the electrical activity changed frequently. After blocking contractions with blebbistatin, the spatiotemporal pattern of electrical activity became less variable and less complex. Under control conditions (no pharmacological agent), stretching (and also releasing) the cardiomyocyte monolayers transiently increased beat rate. Blebbistatin attenuated the acceleration of beating upon stretch. In contrast, streptomycin had no detectable effects. Thus, active force generation is involved in determining beating variability in spontaneously active cardiac tissue. Possible mechanisms may include cellular processes that sense contraction and chemical messengers. Our study contributes to understanding how mechano-electric feedback influences heart rate variability.

Abstract

Cardiomyocyte cultures exhibit spontaneous electrical and contractile activity, as in a natural cardiac pacemaker. In such preparations, beat rate variability exhibits features similar to those of heart rate variability in vivo. Mechanical deformations and forces feedback on the electrical properties of cardiomyocytes, but it is not fully elucidated how this mechano-electrical interplay affects beating variability in such preparations.

Using stretchable microelectrode arrays, we assessed the effects of the myosin inhibitor blebbistatin and the nonselective stretch-activated channel blocker streptomycin on beating variability and on the response of neonatal or foetal murine ventricular cell cultures against deformation. Spontaneous electrical activity was recorded without stretch and upon predefined deformation protocols (5% uniaxial and 2% equibiaxial strain, applied repeatedly for 1 min every 3 min).

Without stretch, spontaneous activity originated from the edge of the preparations, and its site of origin switched frequently in a complex manner across the cultures. Blebbistatin did not change mean beat rate, but it decreased the spatial complexity of spontaneous activity. In contrast, streptomycin did not exert any manifest effects. During the deformation protocols, beat rate transiently increased upon stretch, but paradoxically also upon release. Blebbistatin attenuated the response to stretch, while this response was not affected by streptomycin.

Therefore, our data support the notion that in a spontaneously firing network of cardiomyocytes, active force generation, rather than stretch-activated channels, is mechanistically involved in the complexity of the spatiotemporal patterns of spontaneous activity and in the stretch-induced acceleration of beating.

First author profile

Seyma Nayir is currently a PhD candidate in the Integrative Cardiac Bioelectricity Group led by Professor Jan P. Kucera at the Department of Physiology of the University of Bern. She has a background in Experimental Physics with a Bachelor's and Master's degree from Istanbul Technical University (Turkey). Seyma really enjoys doing technically challenging experiments and she is keen to apply her knowledge to life sciences. Her research focuses on the effects of mechanical deformation (stretch) on cardiac electrical activity.

Introduction

During normal heart rhythm, every heartbeat is initiated by an action potential (AP) that originates in the sinoatrial node (SAN). The AP then propagates through the heart and triggers the contraction of cardiomyocytes (Bers 2002). Irregular or uncoordinated electrical excitation can result in arrhythmias and compromise cardiac output.

The SAN is a network of connected cells that spontaneously generate APs by slow diastolic depolarization that brings the membrane potential to the threshold of voltage-gated inward currents (Noma 1996). Two jointly operating mechanisms, known as the "membrane clock" and the "calcium clock", contribute to this diastolic depolarization (Lakatta & DiFrancesco 2009). The membrane clock relies on the activation of the inward "funny" current carried by hyperpolarization-activated nucleotide-gated cation channels HCN4 (DiFrancesco 2010; Bychkov *et al.* 2020), while the calcium (Ca^{2+}) clock results from the spontaneous release of $Ca^{2+}$from the sarcoplasmic reticulum during late diastole, causing additional inward current via sodium-calcium exchange (Maltsev & Lakatta 2007). In the classical paradigm of SAN function, pacemaker cells synchronize via gap junctional coupling by mutual entrainment, whereby the cells or a group of cells exhibiting the fastest intrinsic rate entrains the other cells of the tissue (Jalife 1984; Verheijck *et al.* 1998).

However, the SAN is a very heterogeneous structure with different patterns of ion channel expression and with an intercellular coupling gradient of different types of connexins (Boyett *et al.* 2000). While connexin 43 (Cx43) is expressed at the periphery of the SAN, it is scarce in its centre, where Cx40 mediates intercellular coupling (Boyett *et al.* 2000). Detailed structural studies have revealed that the SAN is in fact formed by a meshwork of intermingling Cx43 positive and negative strands (Boyett *et al.* 2000; Bychkov *et al.* 2020), whereby the Cx43 positive strands form pathways along which APs are conducted to the surrounding atrium in a discontinuous manner (Bychkov *et al.* 2020). This mingling of Cx43 positive and negative tissue provides a mechanism by which the SAN is able to drive the surrounding atrium, which, by exhibiting a more negative resting membrane potential, tends to suppress pacemaking (Joyner & van Capelle 1986; Boyett *et al.* 2000; Bychkov *et al.* 2020). Recent investigations demonstrated a meshwork of HCN4 positive, F-actin negative and Cx43 negative cells intertwined with a meshwork of HCN4 negative, F-actin positive and Cx43 positive cells (Bychkov *et al.* 2020). At the large interface between both meshworks, these two cellular populations are joined by a very narrow gap (Bychkov *et al.* 2020). This intermeshing extends over the entire SAN, without gradient or mosaic patterns and the HCN4 positive cells exhibit complex shapes (Bychkov *et al.* 2020).

At the functional level, it was shown in the same study (Bychkov *et al.* 2020) that synchronized APs emerge from heterogeneous subcellular subthreshold Ca^{2+} signals (local Ca^{2+} releases) in the HCN4 positive and F-actin negative cellular meshwork. These local Ca^{2+} releases greatly differ in spatial distribution, frequency, amplitude and phase. At the cellular level, patterns of Ca^{2+} signalling range from highly synchronized to less synchronized or irregular. Some SAN cells generate diastolic LCRs preceding full Ca^{2+} transients in adjacent cells, but do not produce full Ca^{2+} transients on their own. The resulting Ca^{2+} signals thus appear discontinuous at a macroscopic scale and the interaction of these Ca^{2+} events leads to a multiscale process of impulse generation. The HCN4 positive cells are

believed to be the region of weakly coupled entrained oscillators and, possibly, only a fraction of HCN4 positive cells participate in AP generation.

Using patch clamp recordings in isolated SAN cells from wild-type mice and a knock-in murine model of HCN4 with defective regulation by cyclic adenosine monophosphate (cAMP), another research group revealed two populations of SAN cells: one population of cells firing APs and another one that switches between a firing and a non-firing mode (Fenske *et al.* 2020). Using Ca^{2+} mapping, the authors correlated these populations with one exhibiting large global Ca^{2+} transients, and the other with only subthreshold local Ca^{2+} signals or Ca^{2+} waves that did not spread to other cells. The proportion of non-firing cells was larger in the knock-in model, indicating that regulation by cAMP is important to bring the cells to fire, and the proportion of the two pools was modulated by agonists and antagonists of the autonomous nervous system (ANS). Based on these findings, the authors proposed that the non-firing cells form an inhibitory cell pool that exerts a tonic depressing effect on the firing cell pool, thus decreasing the rate of the firing cells. Thus, besides classical mutual entrainment (Jalife 1984), SAN activity may also by modulated by this tonic interaction, leading to a new paradigm of chronotropy in which the ANS influences the relative proportion of the firing and non-firing populations (Fenske *et al.* 2020).

At the level of functional integration, the SAN activity thus results from the self-similar organization of local Ca^{2+} signals from the subcellular to the tissue scale, in the form of a process that can be envisioned as fractal-like (Bychkov *et al.* 2020). These findings challenge the view that a dominant centre in the SAN drives pacemaking (Clancy & Santana 2020). Rather, APs emerge from very heterogeneous self-organizing Ca^{2+} events arising in very diverse cell populations that operate in a subthreshold regime and interact via different coupling modalities, which permits rapid entrainment and stochastic resonance (Clancy & Santana 2020). In the critical regime, the signals arising from the Ca^{2+} clock eventually percolate through the SAN (Weiss & Qu 2020) and it has been proposed that this mode of operation confers the SAN a high level of resilience and tunability (Clancy & Santana 2020). Taken together, these studies have provided important insight into the interdependence of the Ca^{2+} and voltage clock mechanisms and the self-organized rhythmic activity of the SAN.

Heart rate is mainly modulated by the autonomic nervous system (ANS). The analysis of the resulting heart rate variability (HRV) is an established method to evaluate ANS function and to derive prognostic markers (Camm & Malik 1996). Interestingly, at very low frequencies, HRV exhibits a power-law behaviour (Akselrod *et al.* 1981; Camm & Malik 1996; Sassi *et al.* 2015), which implies that HRV exhibits statistically self-similar (fractal) properties without any characteristic time scale. It was reported that the exponent of this power-law and related fractal measures (such as the scaling exponent of detrended fluctuation analysis (Peng *et al.* 1995; Behar *et al.* 2018a)) may be of diagnostic or predictive value in the context of cardiac disease (Makikallio *et al.* 2001a; Makikallio *et al.* 2001b; Gang *et al.* 2011). Remarkably, this fractal behaviour is present even in the isolated and denervated heart and in the isolated SAN (Yaniv *et al.* 2014). We have previously demonstrated a power-law behavior of beat rate variability (BRV) in monolayer cultures of neonatal rat ventricular myocytes (Kucera *et al.* 2000; Ponard *et al.* 2007), an in vitro model of a natural cardiac pacemaker, and such fractal behaviour of BRV was also reported in isolated cardiomyocytes (Harada *et al.* 2009) as well as in embryoid bodies of human embryonic and induced pluripotent stem cell-derived cardiomyocytes (Mandel *et al.* 2012). This fractal behaviour of HRV and BRV thus appears to be a universal phenomenon which is, at least in part, mediated by intrinsic dynamic mechanisms at the

tissue and cell levels. It may be caused by fluctuations in ion currents due to their stochastic gating (Wilders & Jongsma 1993), by stochastic local Ca^{2+} releases from the sarcoplasmic reticulum (Monfredi *et al.* 2013) or by spatial and temporal variations of ion channel expression and turnover (Ponard *et al.* 2007). Possibly, criticality and self-organization of single intracellular calcium release events into larger waves contribute to the power law behaviour of BRV by modulating the calcium clock (Nivala *et al.* 2012).

In parallel to the continuous variation of beating rate, cardiac activity is continuously affected by mechanical influences resulting from passive forces and active contractions. The typical example is the Frank-Starling mechanism, which permits, on a beat to beat basis, to adjust and optimize stroke volume to diastolic filling (Lookin & Protsenko 2019). Regarding pacemaker function, it is known that an increase in right atrial pressure causes an increase of heart rate. While the regulation of heart rate, which also contributes to adjusting cardiac output to variations in venous return, involves the ANS (Bainbridge reflex), it is also in part intrinsic to the SAN and mediated by stretch-activated channels (SACs) (Kohl *et al.* 1994; Cooper & Kohl 2005).

The modulation of electrophysiological characteristics by mechanical influences is generally known as mechano-electric feedback (MEF) (Kohl *et al.* 1994; Riemer & Tung 2003; Kamkin *et al.* 2005; Kohl *et al.* 2006; McNary *et al.* 2008; Quinn *et al.* 2014). MEF is most frequently attributed to non-selective SACs (McNary *et al.* 2008; Huang *et al.* 2009), which cause depolarization and triggered activity when activated during diastole (Riemer & Tung 2003; Quinn *et al.* 2017). SACs can be constitutively present in cardiomyocytes or in fibroblasts electrically coupled to myocytes (Kohl *et al.* 1994; Grand *et al.* 2014; Quinn *et al.* 2014). Myocardial stretch also modulates other ion channels directly (McNary & Sachse 2009; Beyder *et al.* 2010) or indirectly by involving the cytoskeleton and intracellular signalling mediators such as nitric oxide (Boycott *et al.* 2020). In addition, MEF can also be mediated by changes in passive tissue resistance (Sachse *et al.* 2004; McNary *et al.* 2008) or capacitance (Mills *et al.* 2008; Pfeiffer *et al.* 2014). Because MEF may cause arrhythmias, it is therefore important, both in physiology and cardiology, to understand the relation between mechanical effects and the excitation of cardiac tissue.

While previous studies mainly focused on passive mechanical influences, the direct involvement of active force generation in MEF has, in comparison, scarcely been investigated. In this context, it was observed in cardiomyocyte cultures that the myosin inhibitor and contraction uncoupler blebbistatin reverts the pro-arrhythmic slowing of conduction induced by co-cultured myofibroblasts (Thompson *et al.* 2011), thereby suggesting that intercellular mechanical junctions (e.g., adherens) between these cells may transmit active forces to mechanosensitive channels (Thompson *et al.* 2014). However, this reversal of conduction slowing was not corroborated in similar experiments by others (Grand *et al.* 2014), suggesting that SACs in the myofibroblasts primarily contribute to stretch-induced conduction slowing. In whole hearts, it was observed that blebbistatin decreases the complexity of ventricular fibrillation (Brines *et al.* 2012). In the setting of pacemaker activity, it was reported that cultured cardiomyocyte monolayers exhibit a higher spatial and temporal instability of spontaneous activation rate when grown on elastic substrates compared to rigid glass (Boudreau-Béland *et al.* 2015). It was also shown that spontaneously beating cardiomyocytes cultured on an elastic substrate can synchronize even without direct contact (no gap junctional coupling) if they are sufficiently close together, and this synchronization is disrupted when active force generation is blocked (Nitsan *et al.* 2016; Viner *et al.* 2019). In the context of the SAN, it is presently debated

whether the HCN4 positive cells communicate exclusively via gap junctions, or whether other factors such as mechanical signalling, chemical signalling (e.g., nitric oxide) or even ephaptic coupling (Ly & Weinberg 2022) are involved (Bychkov *et al.* 2020; Weiss & Qu 2020).

In the present work, to better understand the role of MEF in modulating pacemaker activity, we examined in a first step how the spatiotemporal patterns of spontaneous electrical activity of murine ventricular cell cultures grown on stretchable microelectrode arrays are influenced by blebbistatin and the SAC blocker streptomycin. While these preparations do not mimic the extreme structural and functional complexity of the SAN, they nevertheless recapitulate important hallmarks of pacemaker function, in particular the combination of voltage and calcium clocks (Ponard *et al.* 2007) and the power law behaviour of beat rate variability, which is typical for self-critical and self-organized processes (Kucera *et al.* 2000; Ponard *et al.* 2007; Weiss & Qu 2020). In a second step, we investigated how the response of beat rate to acute stretch is modulated by these two pharmacological agents. Beat rate was transiently increased by stretch, but interestingly also by its release. Blebbistatin decreased the complexity of beating variability and attenuated the increase of beat rate upon stretch. Surprisingly, streptomycin did not exert any detectable effects. Our study thus unveils new roles of active force generation in beating variability and mechano-electrical feedback.

Methods

Ethical approval

Animals were handled in accordance with the ethical principles and guidelines of the Swiss Academy of Medical Sciences. The procuration of animals, the husbandry and the experiments conformed to the European Convention for the Protection of Vertebrate Animals used for Experimental and other Scientific Purposes. The protocols were reviewed and authorized by the Commission of Animal Experimentation of the Cantonal Veterinary Office of the Canton of Bern, Switzerland (authorization number BE36/19), in accordance with Swiss legislation. Experiments were carried out according to the guidelines laid down by the animal welfare committee of the University of Bern, and conformed to the principles and regulations described by Grundy (Grundy 2015).

Stretchable microelectrode arrays

Polydimethylsiloxane (PDMS)-based stretchable microelectrode arrays (sMEAs) were micro-fabricated using a previously published process (Buccarello *et al.* 2018). In brief, 4-inch silicon wafers were spin-coated with poly(4-styrenesulfonic acid) (PSS; 18 wt. % in H_2O; Sigma-Aldrich).

Subsequently, a 0.5 mm thick PDMS base layer was spun onto the wafers. PDMS (Sylgard® 184, Dow Corning) was prepared at a mass ratio of 10:1 of base to curing agent and cured for at least 2 h at 75-80 °C. To prepare electrodes, interconnects and markers for the monitoring of strain (Figure 1A), a first 5 nm chromium layer and a second 35 nm gold layer were thermally evaporated (Auto 306, Edwards) onto the PDMS base layer through a laser-machined polyimide mask. Approximately 10 µm thick encapsulation layers were prepared separately by spinning (5000 rpm for 1 min) PDMS on another 1-2 mm thick PDMS carrier, which was beforehand spin-coated with diluted PSS (9% wt. % in H_2O) and dried at room temperature. After curing, the encapsulation layers were perforated using punchers at the contact sites of the electrodes, and cut into 2x2 cm pieces. The encapsulation layers were then aligned and bonded onto the sMEAs after activation using oxygen plasma. Finally, the wafers carrying the sMEAs were immersed for 2-4 hours in distilled water, whereby the dissolution of PSS led to the spontaneous detachment of the sMEAs from the wafers, as well as of the PDMS carrier layers supporting the encapsulation layers. After drying, the sMEAs were cut into their final shape (see Figure 1A). The electrode layout consisted of 4 stimulation dipoles (diameter: 0.2 mm) and 12 unipolar recording electrodes (diameter: 0.95 mm) separated by 2 mm (Figure 1A).

Murine cardiac cell cultures on sMEAs

Cultures of ventricular myocytes from neonatal (0-1 day post-partum) or foetal (19.5 dpc) wild-type C57BL/6J mice (Charles River) were prepared according to previously published protocols (Beauchamp *et al.* 2004; Prudat & Kucera 2014; Buccarello *et al.* 2018). The animals had ad libitum access to food and water. Neonates were sacrificed by decapitation. To collect foetuses, the mother animal was terminally anesthetized by intraperitoneal injection of xylazine and ketamine (10 mg/kg and 80 mg/kg body mass, respectively). After disappearance of the pedal reflex, the animal was exsanguinated and the uterus was extracted. The foetuses were then collected and sacrificed by decapitation. A total of 56 neonates, 52 foetuses and 11 adult animals were used. The hearts were extracted from the donors and the ventricles were minced to 1 mm-sized pieces. Cardiomyocytes were then dissociated enzymatically using trypsin (0.075%, Gibco) and pancreatin (100 mg/L, Sigma-Aldrich) in Hanks' balanced salts solution (HBSS, Bioconcept) containing phenol red at 37 °C. All cells were pooled together, irrespective of the sex of the animals. Subsequently, the cell suspension was centrifuged, re-suspended in enzyme-free culture medium and pre-plated for 2 h to minimize myofibroblast content. Thereafter, the cells were counted using a Neubauer chamber (Bioswisstech).

In parallel, the sMEAs were preconditioned by oxygen plasma activation and coating with type I collagen (Sigma-Aldrich), diluted at a concentration of 200 mg/L in HBSS (Gibco) containing 12% acetic acid (Grogg Chemie). To generate disk-shaped monolayers, polyimide masks with a circular hole of 8 mm diameter were centred and positioned on the sMEAs electrode layouts (see Figure 1A), and the collagen solution was applied over the masks. To build culture chambers, hollow PDMS cylinders (inner diameter: 17.5 mm; outer diameter: 22 mm; height: 15 mm) were centred and affixed onto the sMEAs using Vaseline. During stretch experiments, this permitted the cylinders to slide on the sMEAs without interfering with their deformation.

After washing the culture substrates with HBSS and sterilizing them using ultraviolet light, the cardiomyocytes were seeded at a density of $1.7 \cdot 10^5/cm^2$ and incubated at 36 °C with 0.9% CO_2. The culture medium (M199 with Hanks' salts (Sigma-Aldrich)) was supplemented with 10% neonatal calf serum (Amimed), 10 mmol/L HEPES (Gibco) and 0.68 mmol/L L-glutamine (Sigma-Aldrich). To prevent bacterial proliferation, the medium was also supplemented with 20 mg/L streptomycin and 20000 U/L penicillin (Biochrom). Of note, the effect of streptomycin as a stretch-activated channel blocker is reversible upon washout (Ninio & Saint 2008). To minimize myofibroblast proliferation, 100 µmol/L bromodeoxyuridine (Sigma-Aldrich) was also added to the medium. After 24 h, the polyimide masks were removed and the culture medium was changed (with 5% instead of 10% neonatal calf serum) to remove non-attached cells. A microphotograph of a culture is shown in Figure 1A.

Stretching system

The stretching system, described in detail previously (Buccarello *et al.* 2018), consisted of four linear motorized stages (MTS25-Z8, Thorlabs) arranged in a symmetric manner along 4 perpendicular directions. The stages carried supports for printed circuit boards (PCBs). These PCBs were attached on the stages using screws (passed through holes punched in the sMEAs, as visible in the left photograph of Figure 1A), and served to clamp the edges of the sMEAs and to interface their connecting pads with a custom-made amplifier array (Kondratyev *et al.* 2007).

Pairwise concurrent operation of the stages permitted to stretch the sMEAs independently along their two main axes (horizontal (*x*) and vertical (*y*) directions in Figure 1A). The markers integrated in the sMEAs were imaged by a camera (B910 HD Webcam, Logitech) positioned underneath. A custom MATLAB (MathWorks) analysis program identified the markers in real time, which permitted to monitor the applied strain by computing the average deformation gradient tensor in the centre of the sMEA and to adjust the strain to the desired target strain using a closed control loop (Buccarello *et al.* 2018). In particular, the system made it possible to apply strictly uniaxial strains in the *x* and *y* directions by precisely compensating the tendency to constriction of an elastic material along axes orthogonal to the main stretch direction.

Electrophysiological experiments

Experiments were conducted 2-3 days after seeding the cultures. To ensure identical conditions in all experiments, the culture medium was first replaced with HBSS (Gibco) pre-warmed to 36 °C. The sMEA was then mounted on the stretching system, and a ring-shaped gold wire was inserted into the bath to serve as ground electrode. The system was then encased in a thermally insulating polystyrene box in which a temperature of 37 °C was maintained with humidified air using a controller (The Cube, Life Imaging Services). A period of 30 min was allowed for equilibration. Unipolar extracellular electrograms from the recording electrodes (Figures 1B and 1C) were

amplified (gain 1000x) and digitized at a sampling rate of 10 kHz and with 12-bit resolution using a data acquisition processor (DAP 4400a, Microstar Laboratories).

For every preparation, a 15-30 min recording of spontaneous electrical activity was first conducted without any mechanical deformation. Subsequently, a second 15 min recording was conducted, during which, every 3 min, 5% uniaxial strain in the *x* direction was applied and maintained for 1 min, followed by release to the undeformed configuration for 2 min; this scheme was repeated 4 or5 times during the recording. Thereafter, a third and a fourth 15-min recording were conducted using the same scheme, but respectively with 5% uniaxial strain in the *y* direction and 2% biaxial strain (i.e., in both directions simultaneously).

Because of the finite speed of the linear stages, completing the full stretch and releasing back to the initial undeformed state took approximately 2 s (uniaxial protocols) and 1.5 s (biaxial protocols). To have precise timestamps of the applied stretches and subsequent releases, electric pulses were generated by the stretch control program at the onset and at the end of every operation of the linear motor stages, and this pulse was fed into an additional data acquisition channel via the audio socket of the computer.

In additional series of experiments, the same entire procedure was repeated after the addition of blebbistatin (10 µmol/L; Sigma-Aldrich) or streptomycin (20 µmol/L; Calbiochem) to the culture bath. Blebbistatin is a myosin II-specific inhibitor that blocks the cross-bridge cycle by binding to an allosteric site in the motor domain of myosin II. It stabilizes an actin-detached state of myosin II, which prevents it from generating force and using ATP (Rauscher *et al.* 2018; Roman *et al.* 2018). We selected blebbistatin because this agent is widely used by the cardiac optical mapping community to suppress motion artefacts (e.g., (Lou *et al.* 2012; Quinn *et al.* 2017; Fenske *et al.* 2020)) and exerts less effects on electrophysiological parameters compared to other agents such as 2,3-butanedione monoxime, diacetyl monoxime or cytochalasin D which are known to modify the cardiac action potential (Baker *et al.* 2004; Brines *et al.* 2012; Lou *et al.* 2012). Streptomycin is an aminoglycoside antibiotic that also blocks non-specific stretch-activated channels (Quinn & Kohl 2021). We selected streptomycin because it is a common pharmacological tool to investigate SACs in cardiac electrophysiology (White 2006; Quinn *et al.* 2017; Quinn & Kohl 2021) and it has been successfully used in cardiac cell culture systems similar to ours (Thompson *et al.* 2011; Grand *et al.* 2014). Other broadly used agents are gadolinium and GsMTx-4. However, gadolinium precipitates in the presence of phosphate and bicarbonate (Quinn & Kohl 2021), precluding its use in the medium that we used for experiments (HBSS). It may also block the sodium current (Quinn & Kohl 2021).

Data analysis

All analyses were conducted using MATLAB. For every recording channel, the signal was first median-filtered (sliding window of 3 samples) to remove occasional single-sample glitches, then filtered using a digital AC coupling filter to remove baseline drift (time constant: 3 ms), and, if the signal-to-noise ratio was low, low-pass filtered using a convolutional Kaiser filter (cut-off frequency 0.5-3 kHz). Activation times were identified as the time points of the minimum of the first derivative,

which was computed using a centred finite-difference scheme. All recordings were inspected and curated manually using a custom MATLAB graphic user interface to correct false negative detections and remove false positives. The user interface permitted to adjust thresholds for detection, whereby the lowest possible threshold was always used to ensure a high sensitivity (low number of false negative detections that needed to be corrected manually) at the expense of a lower specificity (larger number of detections that needed to be deleted manually).

Signals had a typical biphasic shape (see examples in Figures 1B, 1C and 1D), with an initial positive phase, a rapid downstroke lasting typically <1 ms and a negative phase. Because this time course occurs on a time scale shorter than the time constant of the AC filter and because the Kaiser filter involved a symmetric kernel (producing, by design, no phase shifts in the frequency domain), the resulting effect on activation time detection was minimal. Filtering the signal using the Kaiser filter improved the signal-to-noise ratio and thus the proportion of false positive or negative detections that had to be curated manually. Example raw signals, the determination of activation time and the beneficial effects of filtering are illustrated in Figure 1B.

In some traces, the extracellular electrograms were fractionated, i.e., exhibited more than one local minimum of their first derivative. In this case, as illustrated in Figure 1B, corresponding activation times occurring at an interval smaller than a preset value (1 ms) were fused by computing their weighted average, whereby the actual values of the derivative minima were used as weights.

Spontaneous electrical activity manifested as clusters of signals (Figure 1C) with longer intervals between them, reflecting the rapid spread of excitation across the preparations without activity in between. This permitted to unambiguously identify individual spontaneous excitations. To construct Inter-Beat Interval (IBI) time series, the mean activation time series (m_i) was first calculated for every excitation by averaging the activation times at the available electrodes as

$$m_i = \frac{1}{N}\sum_{j=1}^{N} t_{i,j} \ ,$$

where N is the number of electrodes and $t_{i,j}$ is the activation time at electrode j for the i^{th} excitation. Then, the IBI time series was computed as the difference series of m_i.

In the spatial domain, activations typically originated at the periphery of the preparations (see Figure 1D). Due to the limited number of electrodes, it was however not possible to locate the activation focus exactly. Therefore, we resorted to another quantitative marker, which we call slowness, to globally describe the excitation pattern. Slowness is the reciprocal of conduction velocity (de Lange & Kucera 2009) and is expressed in s/cm. In 2 dimensions (or more), slowness can be understood as the spatial gradient of activation time, a vector with the same direction as conduction velocity, but a reciprocal magnitude. For every excitation i, the average slowness $\vec{s_i}$ was computed by least-squares fitting a 2-dimensional linear function to activation time as

$$t_{i,j} = t_{i,0} + s_{i,x}x_j + s_{i,y}y_j \ ,$$

where $t_{i,0}$, $s_{i,x}$ and $s_{i,y}$ are the fit parameters and x_j and y_j are the coordinates of the j^{th} electrode. Slowness was then obtained as

$$\vec{s_i} = \begin{pmatrix} s_{i,x} \\ s_{i,y} \end{pmatrix} .$$

Slowness $\vec{s}$ is related to velocity $\vec{v}$ as $\vec{v} = (1/\|\vec{s}\|^2)\vec{s}$ (Bayly *et al.* 1998; Masè *et al.* 2021; van Schie *et al.* 2021). Our approach is essentially similar to that proposed by Bayly et al. (Bayly *et al.* 1998). Of note, slowness is the primary result of the fitting procedure, whereas velocity is always computed from slowness in a subsequent step (Bayly *et al.* 1998; Masè *et al.* 2021; van Schie *et al.* 2021). A second argument in favour of slowness is that if differences in activation times are small, or, if the excitation pattern is symmetric (e.g., a radially symmetric pattern originating in the centre of the mapped region), overall slowness will be very small (or even 0) and velocity will diverge towards infinity (division by 0) (Bayly *et al.* 1998). The use of slowness permits to avoid this singularity. Figure 1D illustrates activation maps and corresponding slowness vectors.

As an alternative, we used principal component analysis (PCA) to characterize the activation patterns. First, the activation times were offset by mean activation time m_i:

$$t'_{i,j} = t_{i,j} - m_i \ .$$

PCA was then conducted on $t'_{i,j}$. Unless specified otherwise, results are presented in terms of slowness.

The irregularity (complexity) of slowness during a recording of spontaneous activity was quantified using Shannon's entropy (Shannon 1948) of the distribution of the tip of the slowness vector in the *x*-*y* plane. The latter was partitioned into 0.005x0.005 s/cm square bins, and the fraction of data falling into a bin was determined as $p = n/\Sigma n$, where n is the count in the given bin and Σn is the total count over all bins. Entropy E was then calculated as

$$E = -\sum_{i,p_i \neq 0} p_i \ln p_i \ ,$$

where *i* represents the indices of the bins. Distributions that are spread out have a high E, while clustered or localized distributions have a lower E. We used E as a quantitative marker of complexity. Although there exist distinct mathematical methods to quantify complexity (e.g., (Lempel & Ziv 1976)), we use the words "complex" and "complexity" in their literal and intuitive meaning as "complicated, not easy to describe or to understand", as opposed to "simple".

In the time domain, we used detrended fluctuation analysis (DFA) to assess scale-free self-similar, i.e., fractal features (Peng *et al.* 1995; Behar *et al.* 2018b). In brief, the series of IBIs were partitioned into segments of length n. In every segment, the IBIs were first integrated (cumulatively summed), and the resulting series were detrended by least-squares fitting with a linear function. Then, the residual detrended fluctuation DF(n) was computed as the average of the root mean square of all the detrended segments. The procedure was repeated for n going from 4 to 128 in multiplicative steps by $\sqrt{2}$ (n was rounded to the next integer), and the detrended fluctuation exponent α was computed as the linear regression slope of log(DF(n)) vs. log(n). For white noise and Brownian noise, α is 0.5 and 1.5, respectively, whereas for 1/f fractal noise and heart rate variability in vivo, α is near 1 (Peng *et al.* 1995; Behar *et al.* 2018b). DFA was computed using a modified version of the corresponding MATLAB function from the PhysioZoo analysis package (Behar *et al.* 2018b).

Due to beat rate variability, discrete IBI time series are not sampled at constant time intervals. In analyses in which the response of beat rate to a given intervention (stretch or release) was averaged

over repeated interventions, uniformly sampled instantaneous beat rate series were constructed as follows. First, a function of time *f(t)* was defined using the series of mean activation times m_i as

$$f(t) = \frac{1}{m_{i+1} - m_i} \qquad \text{for} \qquad m_i \leq t < m_{i+1} .$$

This function is constant between consecutive m_i's and discontinuous at the m_i's. The instantaneous beat rate series uniformly resampled at constant intervals Δt was then computed as

$$r_i = \frac{1}{\Delta t} \int_{(i-1)\Delta t}^{i\Delta t} f(t)dt .$$

This resampling method offers the advantage that over any time interval, the sum of the corresponding r_i's, multiplied by Δt, always corresponds (up to rounding to the next integer) to the number of interbeat intervals, thus permitting averaging. We used a resampling frequency of 2 Hz (Δt = 0.5 s).

Statistics

Summary data are presented as means ± standard deviations as well as medians with interquartile ranges (IQR). Normality of distributions was assessed using the Shapiro-Wilk test. Normally distributed data were compared using Student's t-test (paired or unpaired, as appropriate). Non-normally distributed data were compared using the Wilcoxon signed rank test. All tests were two-tailed. The threshold for significance was 0.05.

In correlation analyses, the ranks (i.e. quantiles) of the data were correlated instead of the data themselves to obtain Spearman's rank correlation coefficient ρ.

All raw recordings as well as the MATLAB source code of the user interface and scripts generating the panels of Figures 2-8 were deposited on a repository and are openly available (see Data Availability Statement).

Results

Spatiotemporal characterization of spontaneous activity under control conditions

In a first step, we characterized the spatiotemporal patterns of spontaneous electrical activity in disc-shaped monolayer cultures of murine ventricular myocytes grown on stretchable microelectrode arrays (sMEAs) without any mechanical deformation and pharmacologic agent, under control conditions.

Figure 1A shows the design of the sMEAs and illustrates a cardiomyocyte culture. Figure 1B illustrates how activation times were identified. Figure 1C shows an example recording from the 12 unipolar electrodes of the sMEA. The electrograms illustrate the intrinsic variation of the interbeat interval (IBI). For every electrical excitation (i.e., for every cluster of extracellular signals), we described the activation pattern by linear fitting of the measured activation times vs. electrode positions. This fitting procedure yielded an overall slowness vector (which has the same direction as the overall conduction velocity vector, but a reciprocal magnitude). Figure 1D shows electrograms on an expanded time scale and corresponding activation maps of two consecutive activations, together with the slowness vector. Consistent with the findings of a previous study (Ponard *et al.* 2007), spontaneous activity originated from the edge of the preparations and the site of origin switched frequently. This change in originating focus is illustrated in Figure 1D.

The detailed analysis of spontaneous activity in an illustrative experiment is presented in Figure 2. The IBI time series during the 15 minute recording is shown in Figure 2A. The IBI fluctuated irregularly from beat to beat over a wide range, exhibiting occasional sequences with short IBIs as well as longer pauses (one long pause occurred around 145 s with an isolated IBI of 6.07 s; the range of the plot in Figure 2A was limited to 0 to 3 s to better illustrate the IBI fluctuations). Figure 2B shows the *x* and *y* components as well as the norm of the slowness vector for every excitation during the recording and Figure 2C shows the tip of the slowness vector and its trajectory in the *x*-*y* plane. These plots show that the slowness vector exhibited abrupt and irregular changes, indicating that during the recording the origin of the spontaneous electrical excitation changed frequently in a complex manner. As an alternate method to investigate the change in activation pattern, we applied principal component analysis (PCA) of the activation times of every excitation; Figure 2D shows a two-dimensional plot of the first two principal components. In this PCA plot, excitation patterns that are highly correlated are clustered together. Thus, the PCA plot reveals the tendency of the activation patterns to change during the recording. Importantly, the pattern of the PCA plot and of slowness in the *x*-*y* plane are very similar, indicating that the slowness vector was sufficient to describe the activation patterns. This is further supported by Figure 2E, which shows that >95% of the variance was accounted by the first 2 principal components, which is consistent with the 2-dimensionality of the cell cultures. In all experiments together, the first 2 principal components always accounted for >90% of variance. Thus, in the following, we used slowness vectors to describe the activation patterns.

To assess the statistical self-similarity of the IBI series, we used detrended fluctuation analysis (DFA) to obtain the self-similarity exponent α as shown in Figure 2F. Figure 2F represents the root mean square of the detrended fluctuation (DF) versus segment length n in a double logarithmic plot. In this experiment, the slope α of the linear relation between log(DF(n)) and log(n) was 0.76. This value being greater than 0.5 indicates that the IBI variations exhibit statistically self-similar (fractal) properties distinct from random noise, similar to heart rate variability in vivo, for which values near 1 were reported (Peng *et al.* 1995; Behar *et al.* 2018b). The fact that $\alpha<1$ suggests that in vivo, further factors are likely to be involved in shaping heart rate variability.

Figure 2G shows a plot of interbeat slowness differences (computed as the norm of the difference between successive slowness vectors) versus the IBIs themselves, and corresponding quantiles (represented as blue lines). The distribution was not normal and exhibited a cluster with small interbeat changes in slowness, and another cluster with large changes. This plot also shows that

large interbeat slowness differences accounted for about 20% of the data. To further examine the relationship between interbeat slowness change and IBI, we represented the same data in Figure 2H in the form of a quantile-quantile plot. The grayscale map in the background shows the fraction of data within 0.2x0.2 quantile bins normalized by the fraction that would be expected in the absence of any correlation (0.2·0.2=0.04). Values above 1, indicating a positive correlation, were striking in the top right and the bottom left corners of Figure 2H. Spearman's rank correlation coefficient ρ was 0.169. The higher density of data points in these two corners and Spearman's ρ being greater than 0 thus reveals that interbeat slowness difference and IBI were positively correlated. Specifically, larger IBIs were associated to larger interbeat slowness differences, i.e., large changes in the origin of the spontaneous excitation, while smaller IBIs were associated to smaller changes in the activation pattern.

Blebbistatin decreases the spatial complexity of spontaneous electrical activity and breaks down the correlation between IBIs and interbeat slowness differences

To evaluate the involvement of active cardiomyocyte contraction on the spatiotemporal characteristics of the variability of spontaneous electrical activity, we examined the effects of the myosin inhibitor blebbistatin. In these experiments, the analysis in Figure 2 was conducted for 15 minute recordings (without external deformation) before and after the addition of 10 µmol/L blebbistatin to the preparations. Figure 3A shows the analysis of a control recording (different monolayer culture from that in Figure 2) and Figure 3B shows the analysis of the recording with blebbistatin in the same preparation. Of note, we continue to use the term IBI although blebbistatin fully blocked the contraction of the cardiomyocytes, as verified by microscope inspection. Comparison of the IBI series under control conditions and with blebbistatin reveals that larger excursions of IBI disappeared with blebbistatin.

In the spatial domain, abrupt changes of slowness were suppressed by blebbistatin, indicating that the origin of the electrical activation exhibited smaller and less frequent changes compared to control conditions. This was reflected by the more localized distribution of the slowness vector in the *x-y* plane and by the decrease of the entropy E of this distribution from 4.82 to 0.85. The DFA exponent α was 0.96 and 0.85 under control conditions and with blebbistatin, respectively.

The summary analysis of 11 experiments is presented in Figure 3C. The corresponding recordings involved 547±246 activations. Blebbistatin did not manifestly affect the mean IBI and thus the mean beat rate of the preparations (p=0.520, Wilcoxon signed rank test). However, it significantly reduced the entropy of the distribution of the slowness vector (p=0.0293, paired Student's t-test), and thus it decreased the complexity of the variability of the activation pattern. Blebbistatin did not have any effect on the exponent α (p=0.315, paired Student's t-test), indicating that the self-similarity of the IBI series was preserved. Under control conditions, Spearman's ρ was positive in all experiments under control conditions (different from 0 with p=0.000112, one-sample Student's t-test vs. 0), confirming the correlation between the interbeat changes in activation patterns and the IBIs. Interestingly, in the presence of blebbistatin, the values of ρ clustered near 0 (p=0.320, one-sample Student's t-test for a difference from 0), indicating that this correlation disappeared. Thus, in

summary, blebbistatin decreased the spatial complexity of spontaneous activity and the correlation between activation pattern changes and IBIs.

A series of experiments with the same protocol and analysis was conducted to assess the effects of the non-specific stretch-activated channel blocker streptomycin. As shown in Figure 4, streptomycin (20 µmol/L) exerted no significant effects on mean IBI ($p=0.273$, paired Student's t-test), the entropy of the slowness vector distribution ($p= 0.0766$, paired Student's t-test) and the DFA exponent α ($p=0.311$, paired Student's t-test). Furthermore, Spearman's ρ remained positive not only under control conditions ($p=0.0138$, one-sample Student's t-test vs. 0), but also with streptomycin ($p=0.00662$, one-sample Student's t-test vs. 0). These results suggest that the contribution of streptomycin-sensitive stretch-activated channels in determining or influencing beating variability is minor in our preparations.

Stretch and release both transiently increase beat rate

Next, we aimed at investigating the response of our cultures in terms of spontaneous beat rate upon mechanical stretching and subsequent release. Due to the background beat rate variability, the examination of the effects of stretch and release required averaging over repeated measurements. Therefore, during 15 min recordings, a predefined level of strain was applied to the preparations and maintained for 1 min; the preparation was then released for 2 min to its original undeformed configuration, and this protocol was repeated five times. Figure 5 illustrates such an experiment and the corresponding analysis for 5% uniaxial strain applied in the *x* direction (without any pharmacological agent). Figure 5A illustrates a typical experiment with the stretch protocol and the corresponding IBI and instantaneous beat rate (IBR) time series. While the IBI series was irregularly sampled, the IBR series was resampled from the IBI at a constant rate of 2 Hz (the IBR corresponds to the reciprocal of IBI). This approach permitted to align (i.e., offset) the IBR series on the timings of individual stretches and releases (identified as the onset of linear motor stage action). Note also that since the stages had a finite speed, it took about 2 s to complete the stretching process until the target strain was obtained, and the same time to return to the initial undeformed configuration.

The top graph in Figure 5B shows raster plots before and after the 5 stretches. For all stretches, beat rate increased during the stretch phase (between 0 and 2 s). The aligned IBR data (middle graph) show that IBR increased several fold during stretch, reaching a maximum at the end of the stretch phase. This increase was however transient and the IBR returned to its baseline level within about 8 s. The bottom graph of Figure 5B show the same data after normalization of the IBR series to their average value over 5 s before the start of stretch (normalized beat rate).

The same analysis was conducted for the 5 release episodes, as shown in Figure 5C. As visible in the raster plot, release towards the undeformed configuration also increased beat rate, except in the second release episode. A few seconds before that second episode, beat rate increased and decreased spontaneously; such excursions of beat rate are typical of beat rate variability (see, e.g., Figures 2A and 3A). Nevertheless, on average, IBR also increased upon release in a manner similar as upon stretch (albeit to a lesser extent), and this increase also dissipated after a few seconds.

From every individual monolayer culture, the value of normalized beat rate at the end of the stretch or release phase (when beat rate typically reached its maximum) was extracted for all 5 stretches and releases, and these values were then used for the subsequent summary analysis. The averaged series of normalized beat rate (corresponding to the coloured traces in the bottom graphs of Figures 5B and 5C) were also extracted.

Figure 6 shows this summary analysis for 25 pooled preparations. The analysis included preparations that were later exposed to blebbistatin or streptomycin, as all these experiments were conducted under the same conditions. Figure 6A shows the averaged response to stretch (5% uniaxial strain in the *x* direction) and release in the individual preparations, together with the mean response. This mean response confirms that on average, both stretch and release transiently increased beat rate. However, this response exhibited a large variability between the individual preparations.

Moreover, the baseline average beat rate (left graph of Figure 6B) was also variable, ranging between 0.2 and 2 Hz. To examine whether there was a relationship between baseline beat rate and the magnitude of the response to stretch and release, the preparations were ranked from lowest to highest baseline beat rate (computed as the average IBR before the stretch and release interventions). In the middle and right graphs of Figure 6B, the individual normalized IBR changes for stretch and release are shown according to this ranking. While most data points were >1 (representing an increase), there was no significant correlation between average beat rate and the magnitude of the response of IBR to stretch and release.

The summary statistical analysis is shown in Figure 6C. The left graph shows the mean normalized change of IBR upon stretch and release for 5% uniaxial strain in the *x* direction (the data points correspond to the dots shown in Figure 6A). The distributions were not normal, and Wilcoxon signed rank test was therefore used to test for a difference from 1. The median normalized change in beat rate was 2.02 for stretch (IQR: 1.73-2.69, $p=1.23\cdot10^{-5}$, Wilcoxon signed rank test) and 1.42 for release (IQR: 1.03-1.76, p=0.000174, Wilcoxon signed rank test). Thus, both stretch and release significantly increased beat rate. The same statistical analysis was conducted for 5% uniaxial strain in the *y* direction (middle graph), whereby the median normalized change in beat rate was 2.12 (IQR: 1.74-2.95, $p=1.23\cdot10^{-5}$, Wilcoxon signed rank test) and 1.11 (IQR: 1.03-1.66, p=0.000891, Wilcoxon signed rank test) for stretch and release, respectively. The effect of deformation was similar to that with uniaxial strain in the *x* direction, which is consistent with the isotropy of the cell cultures and the symmetry of the sMEAs and the stretching system. Finally, as shown in the rightmost graph in Figure 6C, 2% biaxial strain also increased beat rate upon both stretch (by a factor 1.65, IQR: 1.38 - 2.40, $p=1.23\cdot10^{-5}$, Wilcoxon signed rank test) and release (by a factor 1.04, IQR: 0.99-1.25, p=0.0173, Wilcoxon signed rank test).

Blebbistatin attenuates the increase of beat rate upon stretch

To investigate whether blebbistatin modulates the increase of beat rate upon stretch and release, we conducted a series of experiments with 8 preparations, with which we repeated the same experiments and the same analysis as shown in Figure 5 after adding 10 µmol/L blebbistatin to the

culture bath. Figure 7A shows the normalized change of beat rate upon stretch and release (5% uniaxial strain in the *x* direction) under control conditions and with blebbistatin, for one example preparation. On average over the 5 stretch episodes, the increase of beat rate upon stretch was attenuated by blebbistatin when compared to control conditions. In this preparation, the response of beat rate upon release was also attenuated by blebbistatin. Figure 7B shows the summary analysis for the 8 preparations.

Blebbistatin significantly attenuated the normalized change of beat rate upon stretch from 2.30±0.46 to 1.57±0.34 for 5% uniaxial strain in the *x* direction (p=0.00198, paired Student's t-test), from 2.26±0.62 to 1.36±0.49 for 5% uniaxial strain in the *y* direction (p=0.0251, paired Student's t-test), and from 1.62±0.31 to 1.18±0.32 for 2% biaxial strain (p=0.0450, paired Student's t-test). However, blebbistatin did altogether not significantly change the response of beat rate to release (p=0.126, 0.461 and 0.511 for for 5% uniaxial strain in the *x* direction, *y* direction and 2% biaxial strain, respectively). Of note, blebbistatin could not be washed out (as confirmed after several washouts by the persistent absence of contractions under microscope inspection, see Supplementary Video), and it was thus not possible to assess whether the effect of blebbistatin was reversible.

Finally, using the same approach, we examined in a series with 7 preparations whether streptomycin also modulates the response of beat rate to stretch. As shown in Figure 8 for an example experiment (Figure 8A) and in the summary analysis (Figure 8B), streptomycin did not significantly modify the increase of beat rate upon stretch (p=0.578, 0.367 and 0.844 for for 5% uniaxial strain in the *x* direction, *y* direction and 2% biaxial strain, respectively) and release (p=0.297, 0.313 and 0.563 for for 5% uniaxial strain in the *x* direction (n=7), *y* direction (n=6) and 2% biaxial strain (n=6), respectively). These results thus indicate that the response of beat rate to deformation is modulated by blebbistatin, but that the effect of streptomycin, if any, is minor and undetectable in our experiments.

Discussion

Our main findings can be summarized as follows. In experiments without stretch, we observed that spontaneous electrical activity in our monolayer cultures (8 mm in diameter) originates from the periphery of the preparations with a site of origin prone to abrupt and unpredictable changes. This recapitulates our previous findings (Ponard *et al.* 2007) as well as the observations of others (Boudreau-Béland *et al.* 2015). The DFA exponent was, on average, near 0.65, confirming the presence of long-range temporal correlations and a power-law behaviour of BRV, as we described previously (Kucera *et al.* 2000; Ponard *et al.* 2007). The fact that the DFA exponent was <1 suggests that in vivo, further factors are likely to be involved in shaping HRV. No change of this exponent was detected upon the application of either blebbistatin or streptomycin, suggesting that the fractal behaviour of BRV is not conditioned by active force generation or SACs. However, blebbistatin decreased the complexity of the spatial variability of activation patterns, suggesting that active force generation is mechanistically involved in this variability. Moreover, blebbistatin disrupted the positive correlation between IBIs and the interbeat slowness differences.

In experiments with stretches and releases, repetitions of the stretch-release protocols and averaging demonstrated that stretch increases beat rate. At a first glance, this result appears logical, being in line with previous studies (Kohl *et al.* 1994; Cooper & Kohl 2005) and with the notion that SACs potentiate depolarization during diastole (Riemer & Tung 2003). However, streptomycin had no influence on the response to stretch, while blebbistatin, in contrast, attenuated this response. Furthermore, this increase in beat rate was not sustained but transient and dissipated after a few seconds, suggesting inactivation or desensitization of the stretch-sensing mechanism. In addition, releasing the preparations from strain also increased beat rate. This result is unexpected, because intuitively, one would anticipate that applying the reverse mechanical intervention (release) would cause the opposite effect (slowing of beating), or no effect at all if the stretch-sensing mechanism is desensitized.

Based on experiments in volume loaded ventricles and computational analyses, Mills et al. (Mills *et al.* 2008) suggested that stretch could lead to an increase in membrane capacitance. The subsequent work of Pfeiffer et al. (Pfeiffer *et al.* 2014) indicates that stretch increases the capacitance of cultured ventricular myocytes via recruitment of caveolae to the sarcolemma. Assuming that the number and function of membrane channels and transporters is not affected by stretch, the same ion currents would then have to charge/discharge a larger capacitive load, which is expected to slow both depolarization and repolarization, and thus spontaneous beat rate. However, we did not observe this in our study. As the time course of caveolae incorporation and possible capacitance changes is unknown, we can nevertheless speculate that an increase in capacitance could have contributed to the slow return of beat rate towards baseline after a few seconds. Further studies with dedicated systems, such as the platform developed by De Coulon et al. (de Coulon *et al.* 2021), may provide an appropriate answer in the future.

The mechanisms by which cells sense mechanical cues are exquisitely complex. According to Cox, Bavi and Martinac (Cox *et al.* 2019), ion channels can sense stretch directly via membrane phospholipids (force-from-lipids principle) or indirectly via cytoskeletal proteins or extracellular tethers with which the channels interact (force-from-filaments principle). In the context of our findings, it appears more plausible (if ion channels are involved), that the influence of active force generation is mediated by the force-from-filaments principle. In addition, as reviewed by Prosser and Ward (Prosser & Ward 2014) as well as by Boycott et al. (Boycott *et al.* 2020), mechanical influences can lead to intracellular signalling cascades, leading to modulation of ion channel function by second messengers such as nitric oxide (NO) or extracellular signal-regulated kinase (ERK). More specifically, NO, produced in cardiomyocytes by both endothelial and neuronal NO synthases, is influenced by mechanical forces. In turn, NO impacts on the function of integrins, which link the actin cytoskeleton to the extracellular matrix. NO also influences further cytoskeletal proteins (e.g., talin, vinculin) that are able to sense and integrate mechanical signals. It was suggested that NO stimulation of integrins then promotes NO-mediated Ca^{2+} release from the sarcoplasmic reticulum and modulate the function of L-type Ca^{2+} channels (Boycott *et al.* 2020). In the context of pacemaker function, this would exert repercussion on the Ca^{2+} clock and affect beat rate. To investigate the involvement of NO in mediating the effects of active force on the response to stretch, experiments could be performed in the future in which NO production is depressed by the NO synthase inhibitor L-NAME or enhanced by the NO donor SNAP (Boycott *et al.* 2020) in the presence vs. absence of blebbistatin.

These diverse mechanisms may react not only to passive tension, but also to active forces generated by the cellular contractile apparatus. These intricate mechano-sensing mechanisms are likely to operate jointly and this complex picture must be taken into account in the interpretation of our results. In the following, we will present and discuss a few hypotheses to explain the surprising, unexpected and sometimes paradoxical findings of our study.

Active force generation and the spatiotemporal patterns of pacemaker activity

Let us consider a network of pacemaker cells connected electrically by gap junctions, and assume that individual cells do not have the same intrinsic rate (i.e., the rate they would exhibit if they were disconnected from their neighbours). When coupled, the network synchronizes by mutual entrainment and the activity then originates from a cell or a region of cells having the highest rate (Jalife 1984; Kanakov *et al.* 2007; Ponard *et al.* 2007; Aghighi & Comtois 2017; Gratz *et al.* 2020). This region, by initiating propagated action potentials, then drives the rest of the tissue. Consider now the scenario in which this primary pacemaker region exhibits a decrease of its intrinsic rate (due to intrinsic beat rate variability or, in the intact organism, due to a shift of the sympathovagal balance). In such a situation, another region will take over the primary pacemaking role. This situation arises naturally in the heart when, for example, the atrioventricular node takes over the primary pacemaker role during extreme sinus node bradycardia. In our cultures, this change of pacemaker focus is reflected by a large change in the slowness vector. Conversely, when the primary pacemaker region exhibits an increase of its intrinsic rate, this region will remain the primary pacemaking site and no large change in slowness will be observed. Hence, these considerations explain the positive correlation that we observed between IBIs and interbeat slowness differences.

Curiously, in our experiments, this correlation was disrupted by blebbistatin, indicating that active force generation is involved in the underlying mechanism. This raises the question regarding how active contractions contribute to this phenomenon. Nitsan et al. (Nitsan *et al.* 2016) have shown that the spontaneous beating of isolated cardiomyocytes cultured on polyacrylamide gel can be entrained and synchronized to the oscillating movement of a microprobe inserted into the gel at a short distance of the cell, but not touching it. Remarkably, even after stopping this mechanical stimulation, the myocytes maintained their spontaneous rate close to the rate of the probe movement for up to one hour, indicating that the cells underwent a long-lasting conditioning that permitted them to “learn” this new rate (Nitsan *et al.* 2016). This entrainment was inhibited by the contraction uncouplers butanedione monoxime and blebbistatin, as well as by the microtubule polymerization inhibitor colchicine, but not by the stretch-activated channel blockers gadolinium and GsMTx-4. This entrainment was also observed for two cells located close to each other, but without physical contact (Nitsan *et al.* 2016; Viner *et al.* 2019). As mechanotransduction pathways, the authors proposed a concerted action between microtubules, nitric oxide synthase 2, reactive oxygen species, calmodulin kinase II and ryanodine receptors, which ultimately would regulate calcium release and the calcium clock (Prosser & Ward 2014; Viner *et al.* 2019).

Based on these findings, we postulate that active rhythmic contractions in our preparations also condition the myocytes to develop an intrinsic rate close to that of the primary pacemaking site.

Such conditioning would not be mediated by direct mechanical communication via the growth substrate (because PDMS is orders of magnitude stiffer than polyacrylamide gel) or by mechanical cell-cell junctions, but by the actual contraction wave accompanying every action potential. This would permit conditioning over large distances. Hence, when the primary pacemaking site fails (i.e., its rate decreases), another region, at a potentially remote location, can immediately take over. This mechanism would then explain the correlation between IBIs and slowness differences seen in our experiments and the complex spatial variation of the activation pattern. It would also explain why this correlation and this spatial complexity are decreased by blebbistatin. Under blebbistatin, without active contractions, it becomes then less likely that a remote site takes over the primary pacemaker activity and the number of such sites would be decreased, as observed in our experiments. In this manner, active cell contractions may contribute to the regulation of spontaneous activity in both the temporal and spatial domains.

In short-term optical mapping experiments using a calcium-sensitive dye, Boudreau-Béland et al. (Boudreau-Béland *et al.* 2015) also observed frequent shifts of the pacing focus in neonatal rat ventricular myocyte monolayer cultures grown on PDMS. Upon adrenergic stimulation with isoproterenol, beat rate increased while the number of pacing sites decreased (less spatial variability). On the one hand, our observation that short IBIs are associated with smaller changes in the activation pattern are in line with this finding. On the other hand, isoproterenol, by its inotropic effect, should reinforce the involvement of active contractions and augment the spatial variability of the pacemaking site. Hence, we surmise that the mechanism mediated by active contractions is already fully activated even without additional adrenergic stimulation. Untangling these effects (which could be achieved by experiments with both isoproterenol and blebbistatin) was however not our primary goal.

Active force generation and the response of beat rate to stretch

A finding of interest is that the acceleration of beating upon stretch was not sustained but dissipated after a few seconds. This observation is consistent with the work of Cooper and Kohl (Cooper & Kohl 2005), who also reported a transient increase in the beat rate of guinea-pig sinoatrial tissue. Thus, it appears that the underlying mechanism desensitizes. Curiously, stretching of murine sinoatrial node strips caused a decrease in beat rate, and the authors explained this species difference by the different repolarization dynamics (Cooper & Kohl 2005).

Importantly, in this same work (Cooper & Kohl 2005), streptomycin did not influence the response of beat rate to stretch, and our results are in line with these observations. In contrast, blebbistatin clearly attenuated the stretch-induced increase of beat rate in our experiments. This supports the notion that the modulation of spontaneous beat rate by stretch is not primarily mediated by channels directly activated by stretch (or at least by the family of such channels that are sensitive to streptomycin). Rather, our results lend support to the hypothesis that beat rate modulation is mediated by mechano-sensing mechanisms of another kind, possibly via the force-from-filaments principle, and that this mechanism depends on the active contraction generated by actin-myosin filaments. Irrespective of the mechano-sensing pathway, the function of membrane channels must

in the end be altered in favour of depolarizing currents to produce an acceleration of beating. This could happen via modulation of other ion channels, calcium signalling, or nitric oxide synthesis in the cardiomyocytes. Especially calcium signalling and nitric oxide recently captured the attention of scientists with their contribution to mechano-electrical feedback (Prosser & Ward 2014; Boycott *et al.* 2020).

Why does release also increase beat rate?

A further interesting result was that release also increased beat rate, for which we propose the following explanation. Assuming incompressibility, stretching a three-dimensional object in one direction is necessarily accompanied by a constriction in another direction. In experiments with, e.g., 5% uniaxial strain, our stretching setup compensates the constriction in the *y* direction in the plane of the culture substrate. Thus, the substrate area is increased by 5%. This implies that in the *z* direction (normal to the substrate), the cells are constricted by 5%. A similar consideration applies for 2% equibiaxial strain, whereby the area increases by ~4% and thus a constriction of ~4% occurs in the *z* direction. Upon release, the opposite happens, which implies a stretch in the *z* direction. Although cultured cardiomyocytes typically flatten out on the substrate (Jousset *et al.* 2016), it is nevertheless plausible that another (probably smaller) pool of mechanosensitive proteins could react to this deformation along the *z*-axis upon release. Thus, a first pool may react to stretch before desensitizing, followed by the activation of the other not yet desensitized smaller pool upon release. Therefore, a fortiori, any change in the shape of the cultured tissue may increase beat rate. These considerations also explain why, on average, the increase in beat rate was smaller (but still statistically significant) upon stretch when compared to release.

However, it cannot be excluded that two completely different mechano-sensing mechanisms may be involved upon stretch and upon release. We did not detect any significant difference of the response of beat rate to release prior and after the application of blebbistatin. While the reason for this may be a smaller effect size precluding its detection, it is also possible that two different mechano-sensing pools may have been involved, one modulated by active contraction and the other not.

Is it possible that myofibroblasts caused the observed effects?

In intact cardiac tissue, fibroblasts and myofibroblasts outnumber myocytes and therefore represent an important myocardial component (Rohr 2009; Quinn & Kohl 2021). Earlier work showed that fibroblasts can form connections with myocytes (Quinn *et al.* 2016) and heterocellular communication between myocytes and myofibroblasts in cell cultures is well established (Gaudesius

et al. 2003; Miragoli *et al.* 2006; Miragoli *et al.* 2007). Cardiomyocytes can even form connections with further cell types, such as macrophages (Hulsmans *et al.* 2017). Although we minimized the number of myofibroblasts by preplating the dissociated cells and limited their proliferation with bromodeoxyuridine, we cannot exclude the presence of a residual number of such cells, which would influence the automaticity in our cultures under control conditions and especially upon stretch. Recently, de Coulon et al. (de Coulon *et al.* 2021) reported large stretch-activated inward currents in NIH 3T3 cells, a cell line derived from fibroblasts. Thus, the question arises whether the responses to deformation that we observed may have been caused by myofibroblasts or other cell types.

In co-cultures of myocytes and myofibroblasts, Grand et al. (Grand *et al.* 2014) observed that streptomycin decreases the depolarizing effect of myofibroblasts on myocytes due to constitutively active stretch-activated channels expressed in myofibroblasts. Based on this, if the proportion of myofibroblasts was substantial in our preparations, we would expect that streptomycin would decrease the spontaneous beat rate of our cultures even in the absence of stretch and attenuate the increase of beat rate upon stretch. Neither was observed, suggesting that the role of myofibroblasts in our preparations was minor, if not absent. Of note, cardiac myofibroblasts in culture systems require the presence of serum to survive and experiments with such cells are typically conducted with 1% of neonatal calf serum (Miragoli *et al.* 2007; Thompson *et al.* 2011; Grand *et al.* 2014). Our recordings were conducted in the absence of serum, which further minimizes the possibility that myofibroblasts may have affected our observations.

Clinical implications

In the future, biological pacemakers based on genetically engineered cardiac cells or stem-cell derived cardiomyocytes may serve as an alternative to electronic pacemakers for patients suffering from sinus node bradycardia (Rosen *et al.* 2011). In addition, notable progress has been made in cardiac tissue bioengineering for drug testing and regenerative purposes, e.g. patches to graft after myocardial infarction (Weinberger *et al.* 2017). It is thus important to understand how these types of engineered cells and tissues behave in terms of their propensity to generate normal pacemaker activity (if this is their primary goal), but also ectopic or proarrhythmic activity (in the case of, e.g., ventricular patches). Such engineered tissues may increase their rate of spontaneous activity upon stretch. This may be beneficial in the case of pacemaker tissue, but also deleterious in the case of ventricular tissue constructs, as it may potentiate extrasystoles and thus re-entrant arrhythmias during increased preload. Our results also suggest that the active contractile properties of normal, diseased or engineered myocardium may determine its response to mechanical deformation, an aspect that deserves to be investigated further.

Limitations

It may be argued that contraction elements are scarce or absent in the centre of the SAN and that the role of active force generation is not relevant in that region. However, as shown in the study of Bychkov et al. (Bychkov *et al.* 2020), the SAN consists of highly intertwined F-actin positive and negative tissue. Thus, contractile elements are not completely absent in the centre of the SA node. Moreover, both active contractile and passive elastic forces can be transmitted over a certain distance (several cells) due to the action-reaction principle (Newton's 3rd law). It is possible that the role of active force generation is more prominent at the periphery of the SAN or at its interface to the atria. It may also be argued that the expression of connexin 43 and sodium channels is very low in the SAN centre where the impulse is initiated, in contrast to our monolayer preparations, and this represents a limitation of our culture model in this regard. Ideally, one should conduct a similar study with intact SAN tissue, preferably with SANs of larger mammals. The challenges that we foresee will be to ensure that the contact between the tissue and the sMEA remains tight and that the tissue closely follows the movement of the sMEA upon stretch. These challenges will require further developments in bioengineering.

In our study, we used blebbistatin to block active force generation. Nonetheless, it cannot be excluded that blebbistatin exerts non-specific effects, either directly on ion channels or Ca^{2+} handling proteins, or indirectly by decreasing ATP consumption and the cellular metabolic load. Increased ATP availability may potentiate the function of sarcolemmal and sarcoplasmic pumps, and inhibit the ATP-sensitive potassium current (Swift *et al.* 2021). Decreased metabolic load may modify the function of mitochondria, which are organelles that participate in cardiomyocyte Ca^{2+} homeostasis (Shannon & Bers 2004). These considerations about metabolism will apply to any contraction uncoupler.

In our study, we used streptomycin, which may also block potassium channels and L-type Ca^{2+} channels (Quinn & Kohl 2021). Based on our previous observation that blocking L-type Ca^{2+} channels with nifedipine completely suppresses spontaneous electrical activity in cardiomyocyte cultures (Ponard *et al.* 2007), such a non-specific effect would likely have depressed beat rate in our preparations, which we did not observe. There may also be conditions for which the expression of stretch-activated channels could change, e.g., by streptomycin exposure during the culture period preceding the experiments, which may contribute to the absence of streptomycin effects. However, we found no specific evidence in the literature that streptomycin up- or downregulates the expression of SACs.

Our stretching system allowed only slow stretches (~2 s to reach target strain), with a speed that is lower compared to the strain rates present during the normal heartbeat. Furthermore, our system did not allow a cyclic stretch and relaxation pattern synchronized with the electrical activity. Nevertheless, our stretch patterns mimicked an acute increase in preload, as would typically occur in vivo during any situation with an increased end-diastolic volume, such as increased venous return. Of note, our system permitted accurate control and quantification of the applied strain, thus removing the variability of this factor between individual experiments.

While more spatial detail would have been obtained with optical mapping using a voltage-sensitive dye, our use of stretchable microelectrode arrays circumvented the problem posed by the long-term phototoxic damage inherent to such dyes. Moreover, at present, available optogenetic voltage

reporters are still too slow to permit identification of activation times with sub-millisecond precision, an aspect that was essential in our work.

It was also not possible with our system to apply strains greater than 5% (uniaxial) or 2% (biaxial) due to the frequent loss of electrical conductivity of the gold interconnects at these strain levels. Thus, examination of the effects of larger strains was not possible. Nevertheless, it is remarkable that such low levels of deformation already induce measurable changes in beat rate.

Finally, the question remains open to which extent our results can be extrapolated and translated to the intact heart and the human heart. Our platform, permitting the simultaneous control of strain and recording of electrical activity may nevertheless open avenues with other types of cardiac preparations in the future.

Conclusion

Our results indicate that active force generation mechanistically contributes to the complexity of spatiotemporal excitation patterns of spontaneous pacemaker activity. In addition, both stretch and release, and hence any change of shape, can accelerate beating. Our study points to cellular phenomena operating separately from ion channels directly activated by stretch. Our study thus contributes to understand how mechano-electric feedback may influence beat rate and heart rate variability and suggests that the active contractile properties of normal, diseased or engineered myocardium are essential players in mechano-electric feedback. Recent research has challenged the view that a dominant centre in the SAN drives pacemaking (Clancy & Santana 2020), suggested that the SAN operates as a critical system (Weiss & Qu 2020) and raised the question whether factors others than gap junctional coupling are involved in impulse formation in the SAN (Weiss & Qu 2020). Thus, our results suggest that mechanical mechanisms represent a path worth to explore.

References

Aghighi A & Comtois P (2017). Noise-induced effects on multicellular biopacemaker spontaneous activity: Differences between weak and strong pacemaker cells. *Chaos* **27,** 093927.

Akselrod S, Gordon D, Ubel FA, Shannon DC, Berger AC & Cohen RJ (1981). Power spectrum analysis of heart rate fluctuation: a quantitative probe of beat-to-beat cardiovascular control. *Science* **213,** 220-222.

Baker LC, Wolk R, Choi BR, Watkins S, Plan P, Shah A & Salama G (2004). Effects of mechanical uncouplers, diacetyl monoxime, and cytochalasin-D on the electrophysiology of perfused mouse hearts. *Am J Physiol Heart Circ Physiol* **287,** H1771-1779.

Bayly PV, KenKnight BH, Rogers JM, Hillsley RE, Ideker RE & Smith WM (1998). Estimation of conduction velocity vector fields from epicardial mapping data. *IEEE Trans Biomed Eng* **45,** 563-571.

Beauchamp P, Choby C, Desplantez T, de Peyer K, Green K, Yamada KA, Weingart R, Saffitz JE & Kléber AG (2004). Electrical propagation in synthetic ventricular myocyte strands from germline connexin 43 knockout mice. *Circ Res* **95,** 170-178.

Behar JA, Rosenberg AA, Shemla O, Murphy KR, Koren G, Billman GE & Yaniv Y (2018a). A universal scaling relation for defining power spectral bands in mammalian heart rate variability analysis. *Front Physiol* **9,** 1001.

Behar JA, Rosenberg AA, Weiser-Bitoun I, Shemla O, Alexandrovich A, Konyukhov E & Yaniv Y (2018b). PhysioZoo: a novel open access platform for heart rate variability analysis of mammalian electrocardiographic data. *Front Physiol* **9,** 1390.

Bers DM (2002). Cardiac excitation-contraction coupling. *Nature* **415,** 198-205.

Beyder A, Rae JL, Bernard C, Strege PR, Sachs F & Farrugia G (2010). Mechanosensitivity of $Na_v1.5$, a voltage-sensitive sodium channel. *J Physiol* **588,** 4969-4985.

Boudreau-Béland J, Duverger JE, Petitjean E, Maguy A, Ledoux J & Comtois P (2015). Spatiotemporal stability of neonatal rat cardiomyocyte monolayers spontaneous activity is dependent on the culture substrate. *PLoS One* **10,** e0127977.

Boycott HE, Nguyen MN, Vrellaku B, Gehmlich K & Robinson P (2020). Nitric oxide and mechano-electrical transduction in cardiomyocytes. *Front Physiol* **11,** 606740.

Boyett MR, Honjo H & Kodama I (2000). The sinoatrial node, a heterogeneous pacemaker structure. *Cardiovasc Res* **47,** 658-687.

Brines L, Such-Miquel L, Gallego D, Trapero I, Del Canto I, Zarzoso M, Soler C, Pelechano F, Canoves J, Alberola A, Such L & Chorro FJ (2012). Modifications of mechanoelectric feedback induced by 2,3-butanedione monoxime and blebbistatin in Langendorff-perfused rabbit hearts. *Acta Physiol (Oxf)* **206,** 29-41.

Buccarello A, Azzarito M, Michoud F, Lacour SP & Kucera JP (2018). Uniaxial strain of cultured mouse and rat cardiomyocyte strands slows conduction more when its axis is parallel to impulse propagation than when it is perpendicular. *Acta Physiol (Oxf)* **223,** e13026.

Bychkov R, Juhaszova M, Tsutsui K, Coletta C, Stern MD, Maltsev VA & Lakatta EG (2020). Synchronized cardiac impulses emerge from heterogeneous local calcium signals within and among cells of pacemaker tissue. *JACC Clin Electrophysiol* **6,** 907-931.

Camm AJ & Malik M (1996). Task force of the european society of cardiology and the north american society of pacing and electrophysiology: Heart rate variability: standards of measurement, physiological interpretation, and clinical use. *Eur Heart J* **17,** 354-381.

Clancy CE & Santana LF (2020). Evolving discovery of the origin of the heartbeat: a new perspective on sinus rhythm. *JACC Clin Electrophysiol* **6,** 932-934.

Cooper PJ & Kohl P (2005). Species- and preparation-dependence of stretch effects on sino-atrial node pacemaking. *Ann N Y Acad Sci* **1047,** 324-335.

Cox CD, Bavi N & Martinac B (2019). Biophysical principles of ion-channel-mediated mechanosensory transduction. *Cell Rep* **29,** 1-12.

de Coulon E, Dellenbach C & Rohr S (2021). Advancing mechanobiology by performing whole-cell patch clamp recording on mechanosensitive cells subjected simultaneously to dynamic stretch events. *iScience* **24,** 102041.

de Lange E & Kucera JP (2009). The transfer functions of cardiac tissue during stochastic pacing. *Biophys J* **96,** 294-311.

DiFrancesco D (2010). The role of the funny current in pacemaker activity. *Circ Res* **106,** 434-446.

Fenske S, Hennis K, Rotzer RD, Brox VF, Becirovic E, Scharr A, Gruner C, Ziegler T, Mehlfeld V, Brennan J, Efimov IR, Pauza AG, Moser M, Wotjak CT, Kupatt C, Gonner R, Zhang R, Zhang H, Zong X, Biel M & Wahl-Schott C (2020). cAMP-dependent regulation of HCN4 controls the tonic entrainment process in sinoatrial node pacemaker cells. *Nat Commun* **11,** 5555.

Gang UJ, Jons C, Jorgensen RM, Abildstrom SZ, Messier MD, Haarbo J, Huikuri HV, Thomsen PE & investigators C (2011). Risk markers of late high-degree atrioventricular block in patients with left ventricular dysfunction after an acute myocardial infarction: a CARISMA substudy. *Europace* **13,** 1471-1477.

Gaudesius G, Miragoli M, Thomas SP & Rohr S (2003). Coupling of cardiac electrical activity over extended distances by fibroblasts of cardiac origin. *Circ Res* **93,** 421-428.

Grand T, Salvarani N, Jousset F & Rohr S (2014). Aggravation of cardiac myofibroblast arrhythmogeneicity by mechanical stress. *Cardiovasc Res* **104,** 489-500.

Gratz D, Winkle AJ, Dalic A, Unudurthi SD & Hund TJ (2020). Computational tools for automated histological image analysis and quantification in cardiac tissue. *MethodsX* **7,** 22-34.

Grundy D (2015). Principles and standards for reporting animal experiments in The Journal of Physiology and Experimental Physiology. *J Physiol* **593,** 2547-2549.

Harada T, Yokogawa T, Miyaguchi T & Kori H (2009). Singular behavior of slow dynamics of single excitable cells. *Biophys J* **96,** 255-267.

Huang H, Wang W, Liu P, Jiang Y, Zhao Y, Wei H & Niu W (2009). TRPC1 expression and distribution in rat hearts. *Eur J Histochem* **53,** 217-223.

Hulsmans M, Clauss S, Xiao L, Aguirre AD, King KR, Hanley A, Hucker WJ, Wulfers EM, Seemann G, Courties G, Iwamoto Y, Sun Y, Savol AJ, Sager HB, Lavine KJ, Fishbein GA, Capen DE, Da Silva N, Miquerol L, Wakimoto H, Seidman CE, Seidman JG, Sadreyev RI, Naxerova K, Mitchell RN, Brown D, Libby P, Weissleder R, Swirski FK, Kohl P, Vinegoni C, Milan DJ, Ellinor PT & Nahrendorf M (2017). Macrophages facilitate electrical conduction in the heart. *Cell* **169,** 510-522 e520.

Jalife J (1984). Mutual entrainment and electrical coupling as mechanisms for synchronous firing of rabbit sino-atrial pace-maker cells. *J Physiol* **356,** 221-243.

Jousset F, Maguy A, Rohr S & Kucera JP (2016). Myofibroblasts electrotonically coupled to cardiomyocytes alter conduction: insights at the cellular level from a detailed in silico tissue structure model. *Front Physiol* **7,** 496.

Joyner RW & van Capelle FJ (1986). Propagation through electrically coupled cells. How a small SA node drives a large atrium. *Biophys J* **50,** 1157-1164.

Kamkin A, Kiseleva I, Wagner KD & Scholz H. (2005). Mechano-electric feedback in the heart: evidence from intracellular microelectrode recordings on multicellular preparations and single cells from healthy and diseased tissue. In *Mechanosensitivity in cells and tissues*, ed. Kamkin A & Kiseleva I. Moscow.

Kanakov OI, Osipov GV, Chan CK & Kurths J (2007). Cluster synchronization and spatio-temporal dynamics in networks of oscillatory and excitable Luo-Rudy cells. *Chaos* **17,** 015111.

Kohl P, Bollensdorff C & Garny A (2006). Effects of mechanosensitive ion channels on ventricular electrophysiology: experimental and theoretical models. *Exp Physiol* **91,** 307-321.

Kohl P, Kamkin AG, Kiseleva IS & Noble D (1994). Mechanosensitive fibroblasts in the sino-atrial node region of rat heart: interaction with cardiomyocytes and possible role. *Exp Physiol* **79,** 943-956.

Kondratyev AA, Ponard JG, Munteanu A, Rohr S & Kucera JP (2007). Dynamic changes of cardiac conduction during rapid pacing. *Am J Physiol Heart Circ Physiol* **292,** H1796-H1811.

Kucera JP, Heuschkel MO, Renaud P & Rohr S (2000). Power-law behavior of beat-rate variability in monolayer cultures of neonatal rat ventricular myocytes. *Circ Res* **86,** 1140-1145.

Lakatta EG & DiFrancesco D (2009). What keeps us ticking: a funny current, a calcium clock, or both? *J Mol Cell Cardiol* **47,** 157-170.

Lempel A & Ziv J (1976). On the complexity of finite sequences. *IEEE Trans Inf Theory* **22,** 75-81.

Lookin O & Protsenko Y (2019). Length-dependent activation of contractility and Ca-transient kinetics in auxotonically contracting isolated rat ventricular cardiomyocytes. *Front Physiol* **10,** 1473.

Lou Q, Li W & Efimov IR (2012). The role of dynamic instability and wavelength in arrhythmia maintenance as revealed by panoramic imaging with blebbistatin vs. 2,3-butanedione monoxime. *Am J Physiol Heart Circ Physiol* **302,** H262-269.

Ly C & Weinberg SH (2022). Automaticity in ventricular myocyte cell pairs with ephaptic and gap junction coupling. *Chaos* **32,** 033123.

Makikallio TH, Huikuri HV, Hintze U, Videbaek J, Mitrani RD, Castellanos A, Myerburg RJ & Moller M (2001a). Fractal analysis and time- and frequency-domain measures of heart rate variability as predictors of mortality in patients with heart failure. *Am J Cardiol* **87,** 178-182.

Makikallio TH, Huikuri HV, Makikallio A, Sourander LB, Mitrani RD, Castellanos A & Myerburg RJ (2001b). Prediction of sudden cardiac death by fractal analysis of heart rate variability in elderly subjects. *J Am Coll Cardiol* **37,** 1395-1402.

Maltsev VA & Lakatta EG (2007). Normal heart rhythm is initiated and regulated by an intracellular calcium clock within pacemaker cells. *Heart Lung Circ* **16,** 335-348.

Mandel Y, Weissman A, Schick R, Barad L, Novak A, Meiry G, Goldberg S, Lorber A, Rosen MR, Itskovitz-Eldor J & Binah O (2012). Human embryonic and induced pluripotent stem cell-derived cardiomyocytes exhibit beat rate variability and power-law behavior. *Circulation* **125,** 883-893.

Masè M, Cristoforetti A, Del Greco M & Ravelli F (2021). A divergence-based approach for the identification of atrial fibrillation focal drivers from multipolar mapping: a computational study. *Front Physiol* **12,** 749430.

McNary TG & Sachse FB (2009). Modeling effects of strain-modulated membrane capacitance and conductance of K+ inward rectifier on conduction velocity in cardiac tissue. *IEEE Comp Cardiol* **36,** 381-384.

McNary TG, Sohn K, Taccardi B & Sachse FB (2008). Experimental and computational studies of strain-conduction velocity relationships in cardiac tissue. *Prog Biophys Mol Biol* **97,** 383-400.

Mills RW, Narayan SM & McCulloch AD (2008). Mechanisms of conduction slowing during myocardial stretch by ventricular volume loading in the rabbit. *Am J Physiol Heart Circ Physiol* **295,** H1270-H1278.

Miragoli M, Gaudesius G & Rohr S (2006). Electrotonic modulation of cardiac impulse conduction by myofibroblasts. *Circ Res* **98,** 801-810.

Miragoli M, Salvarani N & Rohr S (2007). Myofibroblasts induce ectopic activity in cardiac tissue. *Circ Res* **101,** 755-758.

Monfredi O, Maltseva LA, Spurgeon HA, Boyett MR, Lakatta EG & Maltsev VA (2013). Beat-to-beat variation in periodicity of local calcium releases contributes to intrinsic variations of spontaneous cycle length in isolated single sinoatrial node cells. *PLoS One* **8,** e67247.

Ninio DM & Saint DA (2008). The role of stretch-activated channels in atrial fibrillation and the impact of intracellular acidosis. *Prog Biophys Mol Biol* **97,** 401-416.

Nitsan I, Drori S, Y.E. L, Cohen S & Tzlil S (2016). Mechanical communication in cardiac cell synchronized beating. *Nat Physics* **12,** 472-478.

Nivala M, Ko CY, Nivala M, Weiss JN & Qu Z (2012). Criticality in intracellular calcium signaling in cardiac myocytes. *Biophys J* **102,** 2433-2442.

Noma A (1996). Ionic mechanisms of the cardiac pacemaker potential. *Jpn Heart J* **37,** 673-682.

Peng CK, Havlin S, Stanley HE & Goldberger AL (1995). Quantification of scaling exponents and crossover phenomena in nonstationary heartbeat time series. *Chaos* **5,** 82-87.

Pfeiffer ER, Wright AT, Edwards AG, Stowe JC, McNall K, Tan J, Niesman I, Patel HH, Roth DM, Omens JH & McCulloch AD (2014). Caveolae in ventricular myocytes are required for stretch-dependent conduction slowing. *J Mol Cell Cardiol* **76,** 265-274.

Ponard JG, Kondratyev AA & Kucera JP (2007). Mechanisms of intrinsic beating variability in cardiac cell cultures and model pacemaker networks. *Biophys J* **92,** 3734-3752.

Prosser BL & Ward CW (2014). Mechano-chemo transduction tunes the heartstrings. *Sci Signal* **7,** pe7.

Prudat Y & Kucera JP (2014). Nonlinear behaviour of conduction and block in cardiac tissue with heterogeneous expression of connexin 43. *J Mol Cell Cardiol* **76,** 46-54.

Quinn TA, Camelliti P, Rog-Zielinska EA, Siedlecka U, Poggioli T, O'Toole ET, Knopfel T & Kohl P (2016). Electrotonic coupling of excitable and nonexcitable cells in the heart revealed by optogenetics. *Proc Natl Acad Sci U S A* **113,** 14852-14857.

Quinn TA, Jin H, Lee P & Kohl P (2017). Mechanically induced ectopy via stretch-activated cation-nonselective channels Is caused by local tissue deformation and results in ventricular fibrillation if triggered on the repolarization wave edge (commotio cordis). *Circ Arrhythm Electrophysiol* **10**.

Quinn TA & Kohl P (2021). Cardiac mechano-electric coupling: acute effects of mechanical stimulation on heart rate and rhythm. *Physiol Rev* **101,** 37-92.

Quinn TA, Kohl P & Ravens U (2014). Cardiac mechano-electric coupling research: fifty years of progress and scientific innovation. *Prog Biophys Mol Biol* **115,** 71-75.

Rauscher AA, Gyimesi M, Kovács M & Málnási-Csizmadia A (2018). Targeting myosin by blebbistatin derivatives: optimization and pharmacological potential. *Trends Biochem Sci* **43,** 700-713.

Riemer TL & Tung L (2003). Stretch-induced excitation and action potential changes of single cardiac cells. *Prog Biophys Mol Biol* **82,** 97-110.

Rohr S (2009). Myofibroblasts in diseased hearts: new players in cardiac arrhythmias? *Heart Rhythm* **6,** 848-856.

Roman BI, Verhasselt S & Stevens CV (2018). Medicinal chemistry and use of myosin II Inhibitor (S)-blebbistatin and its derivatives. *J Med Chem* **61,** 9410-9428.

Rosen MR, Robinson RB, Brink PR & Cohen IS (2011). The road to biological pacing. *Nat Rev Cardiol* **8,** 656-666.

Sachse FB, Steadman BW, JH BB, Punske BB & Taccardi B (2004). Conduction velocity in myocardium modulated by strain: measurement instrumentation and initial results. *Conf Proc IEEE Eng Med Biol Soc* **5,** 3593-3596.

Sassi R, Cerutti S, Lombardi F, Malik M, Huikuri HV, Peng CK, Schmidt G & Yamamoto Y (2015). Advances in heart rate variability signal analysis: joint position statement by the e-Cardiology ESC Working Group and the European Heart Rhythm Association co-endorsed by the Asia Pacific Heart Rhythm Society. *Europace* **17,** 1341-1353.

Shannon CE (1948). A mathematical theory of communication. *Bell Syst Tech J* **27,** 379-423.

Shannon TR & Bers DM (2004). Integrated Ca2+ management in cardiac myocytes. *Ann N Y Acad Sci* **1015,** 28-38.

Swift LM, Kay MW, Ripplinger CM & Posnack NG (2021). Stop the beat to see the rhythm: excitation-contraction uncoupling in cardiac research. *Am J Physiol Heart Circ Physiol* **321,** H1005-H1013.

Thompson SA, Blazeski A, Copeland CR, Cohen DM, Chen CS, Reich DM & Tung L (2014). Acute slowing of cardiac conduction in response to myofibroblast coupling to cardiomyocytes through N-cadherin. *J Mol Cell Cardiol* **68,** 29-37.

Thompson SA, Copeland CR, Reich DH & Tung L (2011). Mechanical coupling between myofibroblasts and cardiomyocytes slows electric conduction in fibrotic cell monolayers. *Circulation* **123,** 2083-2093.

van Schie MS, Heida A, Taverne Y, Bogers A & de Groot NMS (2021). Identification of local atrial conduction heterogeneities using high-density conduction velocity estimation. *Europace* **23,** 1815-1825.

Verheijck EE, Wilders R, Joyner RW, Golod DA, Kumar R, Jongsma HJ, Bouman LN & van Ginneken AC (1998). Pacemaker synchronization of electrically coupled rabbit sinoatrial node cells. *J Gen Physiol* **111,** 95-112.

Viner H, Nitsan I, Sapir L, Drori S & Tzlil S (2019). Mechanical communication acts as a noise filter. *iScience* **14,** 58-68.

Weinberger F, Mannhardt I & Eschenhagen T (2017). Engineering cardiac muscle tissue: a maturating field of research. *Circ Res* **120,** 1487-1500.

Weiss JN & Qu Z (2020). The sinus node: still mysterious after all these years. *JACC Clin Electrophysiol* **6,** 1841-1843.

White E (2006). Mechanosensitive channels: therapeutic targets in the myocardium? *Curr Pharm Des* **12,** 3645-3663.

Wilders R & Jongsma HJ (1993). Beating irregularity of single pacemaker cells isolated from the rabbit sinoatrial node. *Biophys J* **65,** 2601-2613.

Yaniv Y, Ahmet I, Liu J, Lyashkov AE, Guiriba TR, Okamoto Y, Ziman BD & Lakatta EG (2014). Synchronization of sinoatrial node pacemaker cell clocks and its autonomic modulation impart complexity to heart beating intervals. *Heart Rhythm* **11,** 1210-1219.

Additional information

Data availability statement

All raw recordings as well as the MATLAB source code of the user interface and scripts generating the panels of Figures 2-8 are openly available on the repository Zenodo (https://doi.org/10.5281/zenodo.6524580).

Competing interests

The authors have no competing interests to disclose.

Author contributions

J.P.K. designed the study. S.N. conducted the experiments. S.N. and J.P.K. analysed the data. S.N. prepared the figures. S.N., S.P.L. and J.P.K. drafted the manuscript. All authors approved the final version of the manuscript.

The experiments were performed at the Department of Physiology of the University of Bern.

All authors approved the final version of the manuscript, agreed to be accountable for all aspects of the work in ensuring that questions related to the accuracy or integrity of any part of the work are appropriately investigated and resolved, and all persons designated as authors qualify for authorship, and all those who qualify for authorship are listed.

Funding

This work was supported by the Swiss National Science Foundation (grant n° 310030_184707 to J.P.K).

Acknowledgments

We are grateful to Helene Hinnen for her assistance with the cardiomyocyte cultures, Michael Känzig for taking care of our animals, Michael Stoeckel, Anthony Guillet and the entire cleanroom staff at Geneva Campus Biotech for their training, support and advice, to Ange Maguy for his suggestions on statistics and for proofreading our manuscript, and to Lucilla Giammarino for her support with the video recording.

Translational perspective

Cardiomyocyte cultures are spontaneously active and thus represent a model of a natural cardiac pacemaker. In such cultures, beat rate variability exhibits features similar to those of heart rate variability in vivo. It is however not fully elucidated how mechano-electrical feedback affects beating variability in such preparations. Using stretchable microelectrode arrays, we investigated how the myosin inhibitor blebbistatin and the nonselective stretch-activated channel blocker streptomycin affect beating variability and the response of the beat rate of these cultures to stretch. We found that blebbistatin decreases the spatial complexity of spontaneous electrical activity and attenuates the increase of beat rate caused by stretch. Interestingly, streptomycin exerted no manifest effects. This supports the notion that active force generation, rather than stretch-activated channels, is mechanistically involved in the complexity of spontaneous beating patterns and in the stretch-induced acceleration of beating. In the future, biological pacemakers based on genetically engineered cardiac cells or stem-cell derived cardiomyocytes may serve as an alternative to electronic pacemakers. Moreover, cardiac tissue bioengineering for drug testing and regenerative purposes is constantly progressing. In this context, our study contributes to understanding how these types of engineered cells and tissues behave in terms of their propensity to generate normal pacemaker activity, but also ectopic or pro-arrhythmic activity. Importantly, our results suggest that the active contractile properties of normal, diseased or engineered myocardium may determine its response to mechanical deformation. Finally, our study also suggests that active force generation may influence heart rate variability.

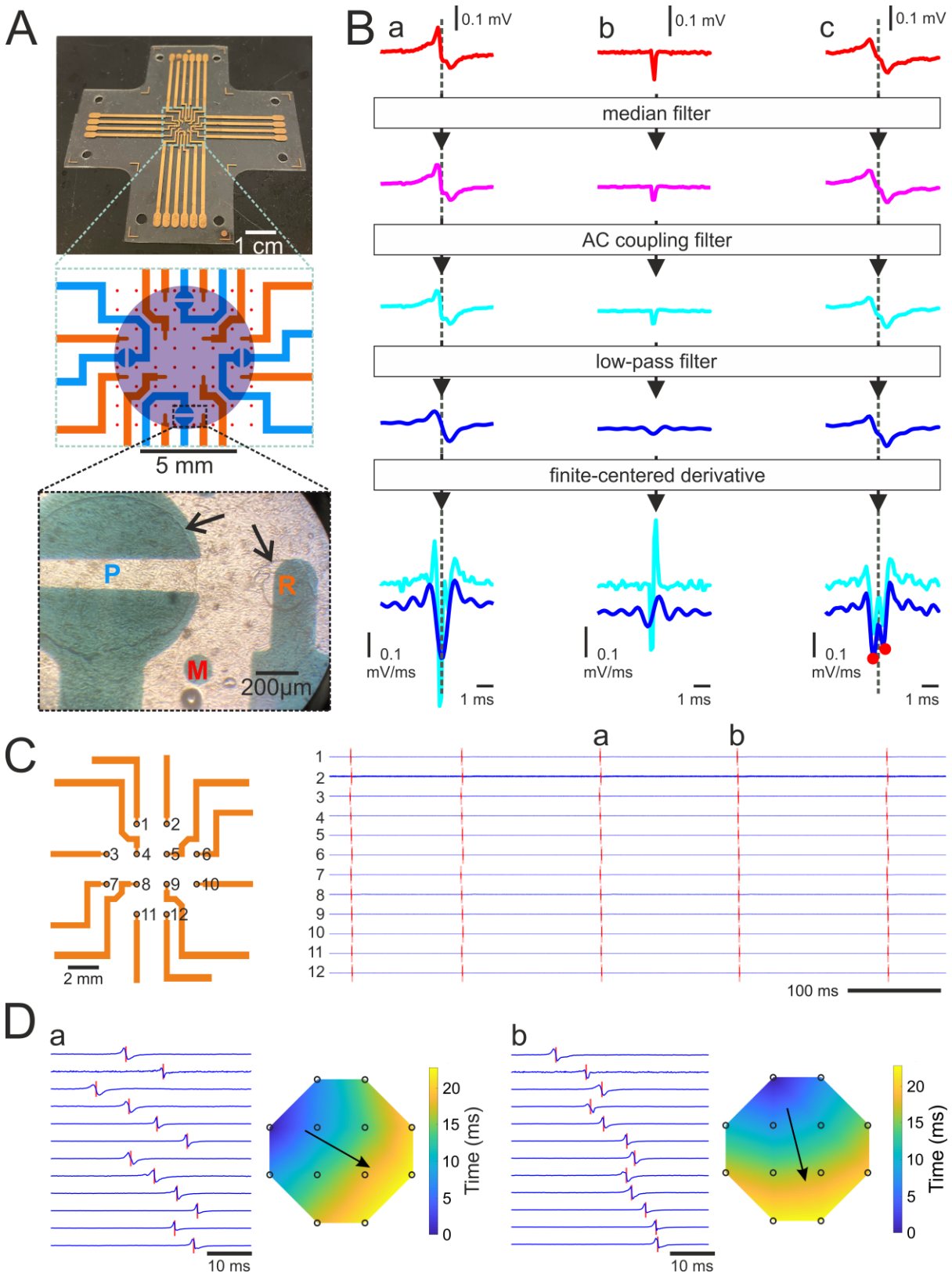

Figure 1. Murine ventricular cardiomyocyte cultures on stretchable microelectrode arrays (sMEAs) and example electrograms.

A: Photograph of a sMEA (top), with its schematic layout (middle). Blue: pacing dipoles; orange: recording electrodes; red: markers for strain monitoring. The area where cells are seeded is shown as a purple disc. The bottom panel shows a photograph of a culture on a sMEA. P: pacing dipole, R: recording electrode; M: marker.

The borders of the encapsulation layer are visible as circles (black arrows). B: Illustration of signal processing for a typical electrogram (a), an artefact resulting from an external perturbation (b) and a fractionated electrogram with two phases in its downstroke (c). Red: raw signals; magenta: after median filtering; cyan: after AC coupling; blue: after low-pass filtering. Bottom: Derivatives of the signals before (cyan) and after (blue) low-pass filtering. Activation time is defined at the minimum of the derivative (grey line in a). Differentiation of the signal in (c) resulted in two negative peaks of the derivative separated by < 1 ms, and activation time was defined as the weighted average of their corresponding timings (red dots), whereby the amplitude of the derivative peaks were used as weights. The artefact in (b) was identified as a false positive based on its clearly different time course. C: Extracellular electrograms recorded by the set of 12 electrodes (schematic and numbering on the left). Activation times are marked with red bars. D: Electrograms and corresponding activation maps of two consecutive activations (a and b, as also labelled in panel B). The black arrows show the main direction of propagation, as calculated from the overall slowness vector (0.0341 and 0.0334 s/cm for a and b, corresponding to average conduction velocities of 29.3 and 29.9 cm/s, respectively). In B and C, the signals were normalized to their amplitude.

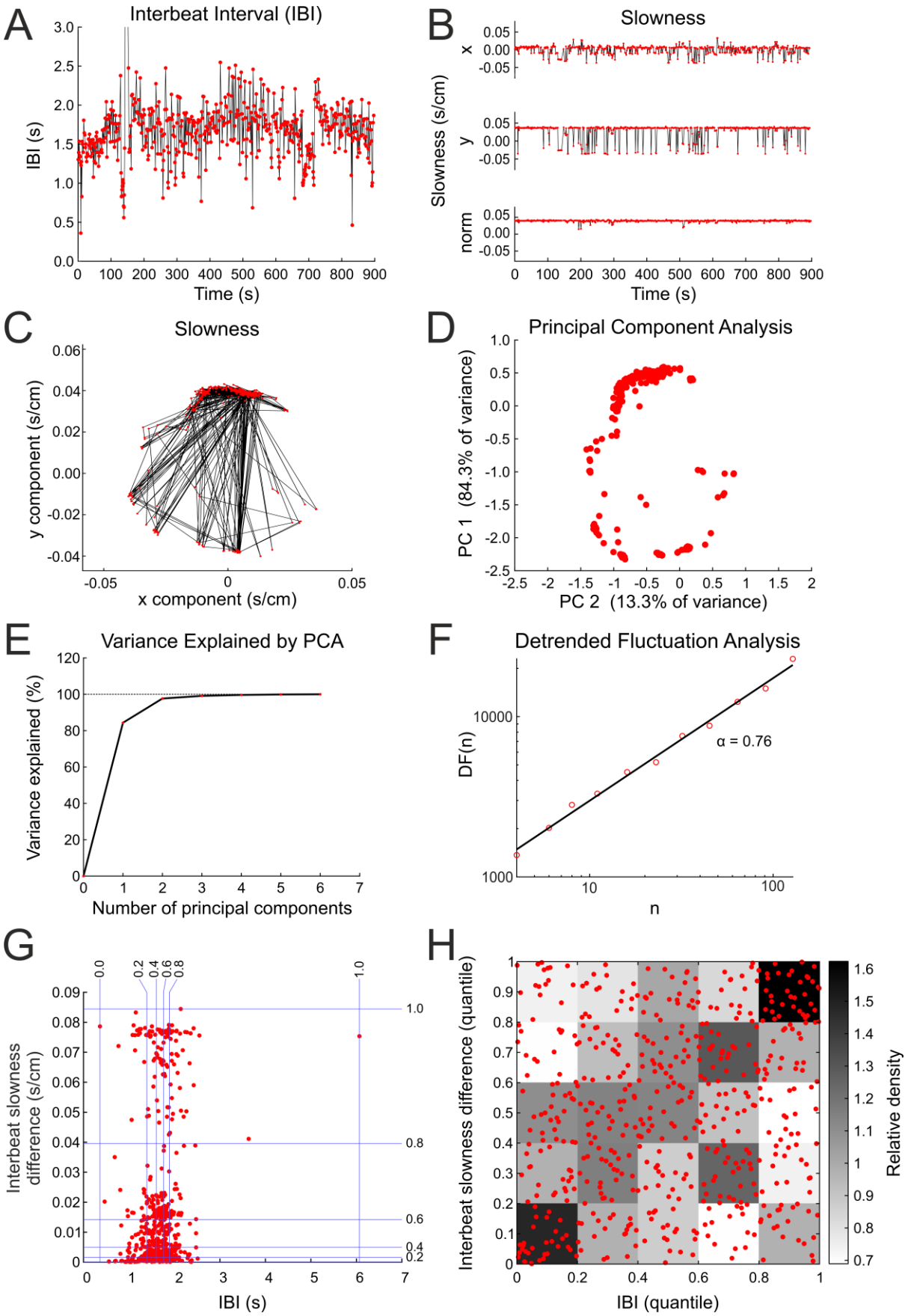

Figure 2. Analysis of beating variability in one example preparation without pharmacological intervention or mechanical deformation.

A: Interbeat interval (IBI) time series for a 15-minute recording. B: *x* and *y* components and norm of the slowness vector for every activation. C: Tip of the slowness vector (red dots) in the *x*-*y* plane. Black lines connect successive vector tips. D: Principal component analysis (PCA) of the activation times of every excitation. E: Cumulated variance explained by PCA as a function of the number of principal components. F: Detrended fluctuation analysis (DFA) plot for the IBI time series. n: length of the detrending segments; DF(n): detrended fluctuation for segments of length n. α: regression slope of DF(n) vs. n on a double logarithmic scale. G: Plot of interbeat slowness differences vs. IBIs. The blue lines denote the 0, 0.2, 0.4, 0.6, 0.8 and 1.0 quantiles. H: Spearman correlation analysis between interbeat slowness difference and IBI (same data as in G, but plotted in terms of quantiles). The relative density was computed for every rectangle as the ratio of the effective number of data points to the number that would be expected without correlation. The Spearman's rank correlation coefficient ρ was 0.169.

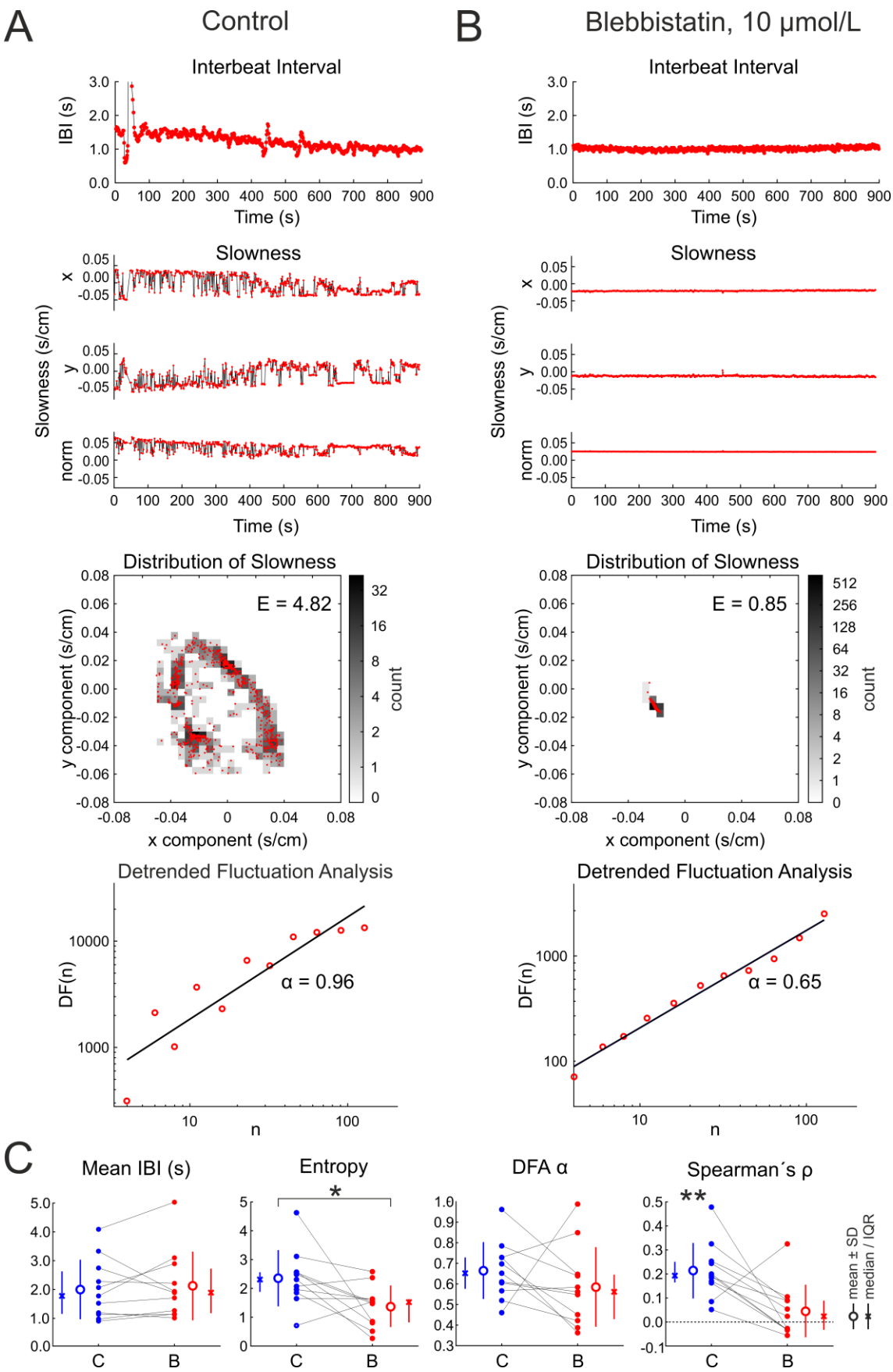

Figure 3. Effects of 10 µmol/L blebbistatin on the spatiotemporal characteristics of excitation variability (without external deformation).

A: From top to bottom: IBI time series, *x* and *y* components and norm of the slowness vector for every activation, distribution of the tips of the slowness vectors in the *x*-*y* plane (red dots) with 2-dimensional histogram (grayscale), and DFA plot, for a preparation under control conditions. B: Same as A, for the same preparation after application of blebbistatin. C: Comparison of mean IBI, entropy of the slowness distribution, DFA exponent α and Spearman's ρ (same analysis an in Figure 2H) under control conditions (label "C") vs. with blebbistatin (label "B"). *: p<0.05 (paired Student's t-test); **: p<0.05 to be positive (Student's t-test). n=11 different monolayer preparations obtained from 8 litters.

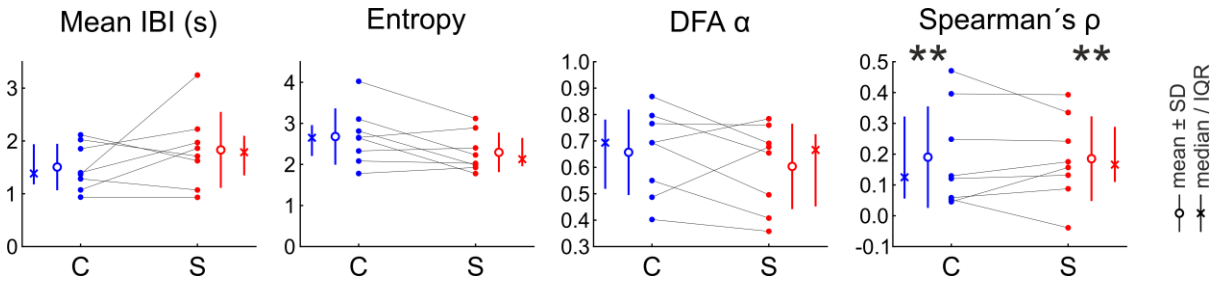

Figure 4. Summary analysis of spatiotemporal characteristics of excitation variability (without external deformation) for the experiments with streptomycin (20 µmol/L).

Comparison of mean IBI, entropy of the slowness distribution, DFA exponent α and Spearman's ρ under control conditions (label "C") vs. with streptomycin (label "S"). p>0.05 for mean IBI, entropy and DFA α (paired Student's t-test). **: p<0.05 to be positive (Student's t-test). n=8 different monolayer preparations obtained from 6 litters. Same layout as Figure 3C.

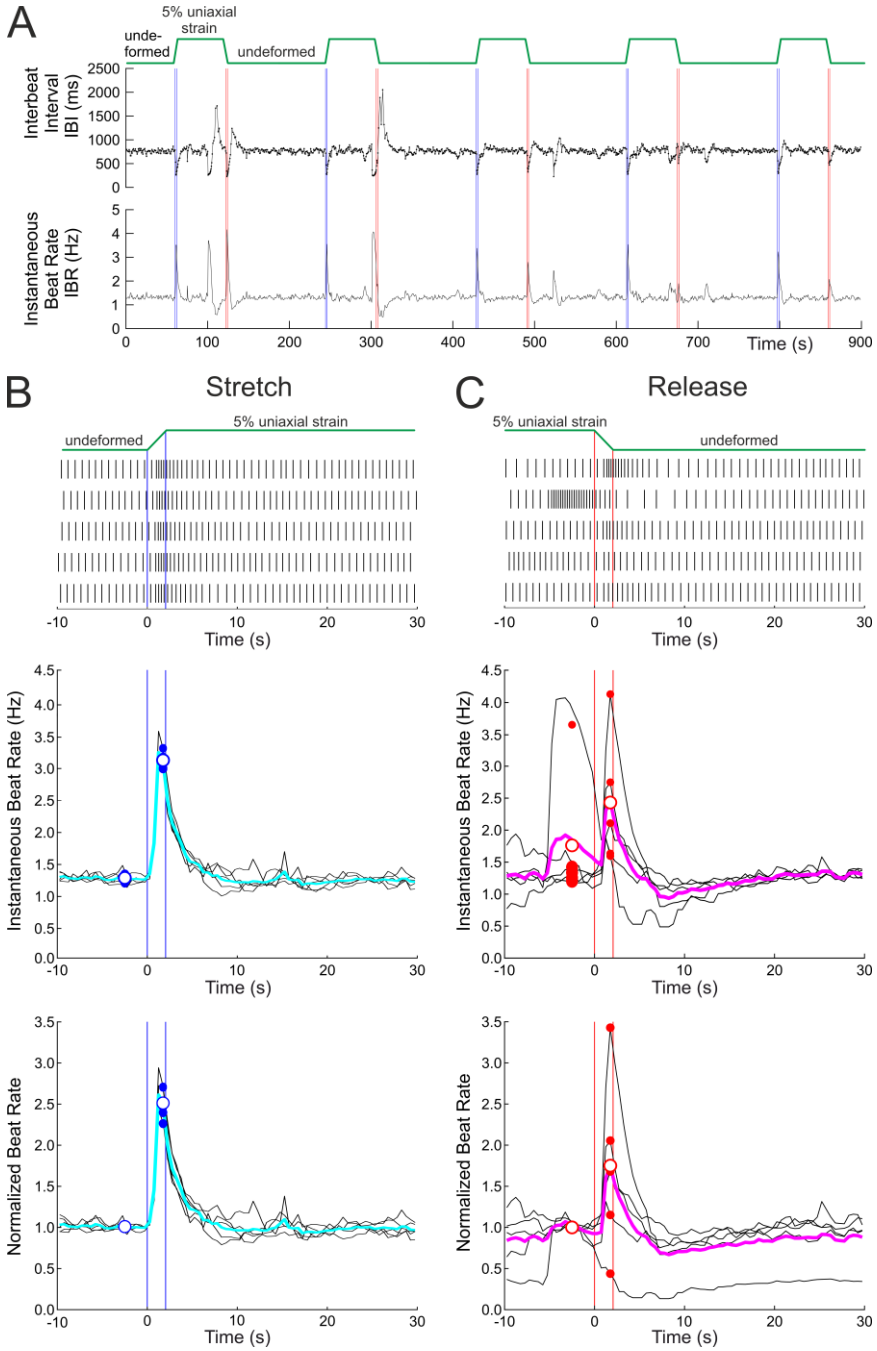

Figure 5. Spontaneous beat rate in an example preparation subjected repeatedly to 5% uniaxial strain.
A: IBI series and corresponding instantaneous beat rate (IBR) for a 15 min recording during which 5% uniaxial strain was repeatedly applied and held for 1 min in the *x* direction (protocol on top). The pairs of lines indicate the start and stop of the linear motors upon stretch (blue) and release (red). B: Top: Raster plot of electrical activations 10 s before and 30 s after each individual stretch (protocol on top), aligned on motor start and end (vertical lines). Middle: Corresponding IBR (black: individual stretches; cyan: average). The small dots at t=–2.5 s represent the average beat rate during the 5 last seconds before stretch and the open circle is the average of these values. The small dots at t=1.75 s represent the IBR at the end of the stretching phase and the open circle is the average of these values. Bottom: Same IBR data, but normalized to the average IBR during the 5 last seconds before stretch. Time is offset to 0 at motor start. The time scale is identical for all plots. C: Same analysis and representation as in B, but for 10 s before and 30 s after each individual release and a different colour coding (magenta and red instead of cyan and blue, respectively).

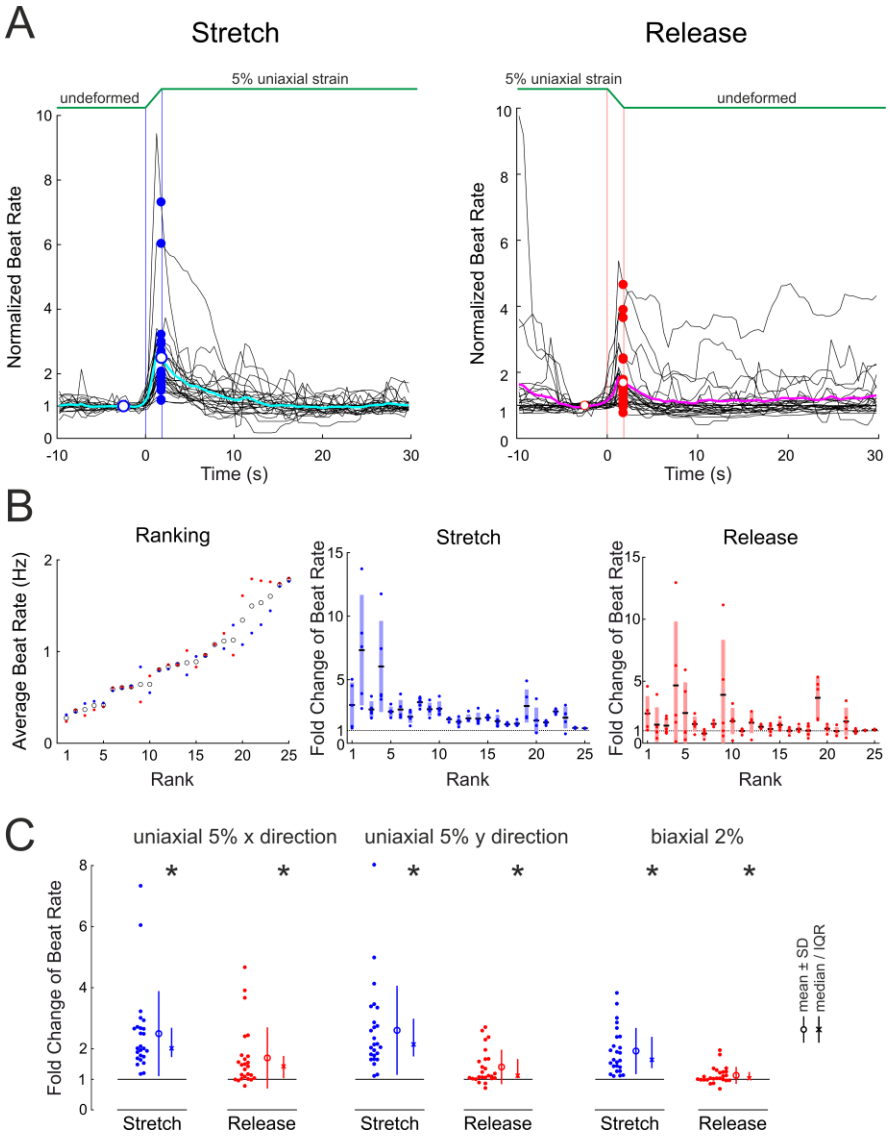

Figure 6. Effects of stretch and release on spontaneous beat rate (without any pharmacological agent).

A: Normalized average beat rate time series for 25 experiments upon stretch (left) and release (right) for uniaxial 5% strain in the *x* direction. The black traces represent the average normalized beat rate series in individual preparations. The coloured traces are the averages for the 25 experiments for stretch and release, respectively. Vertical lines indicate the onset and end of the linear stage movement. The open circles at t=–2.5 s represent the average normalized beat rate before stretch and release (by definition 1). The coloured dots at t=1.75 s represent the mean normalized (peak) increase in individual preparations while the open circle marks the mean of all these values. B: Left: Ranking of the experiments according to their average beat rate in the undeformed position. The blue dots are the average beat rates just before the stretches and the red dots are the average beat rates just before the releases. The black circles are the averages of these two values and served to rank the preparations. Middle: For the corresponding rank, the graphs report the 5 normalized increases of beat rate upon stretch (coloured dots), the corresponding means (black horizontal bars) and standard deviations (pale-coloured bars). Right: same analysis as in the middle panel, but for releases. C: Average normalized (fold) change of instantaneous beat rate (values >1 indicate an increase) in the 25 preparations (obtained from 16 litters) upon stretch and release, for 3 different strain protocols. *: p<0.05, Wilcoxon signed rank test.

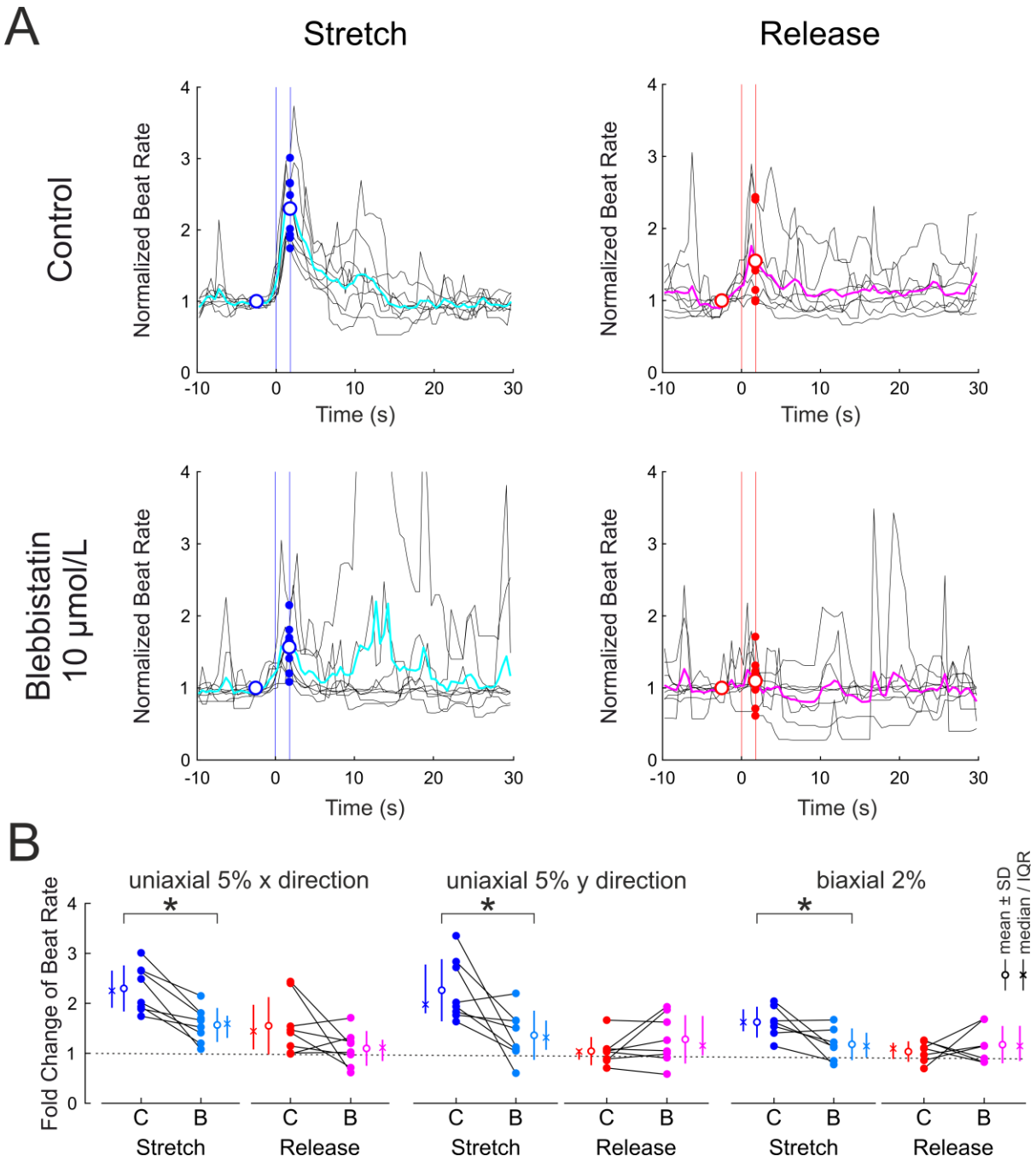

Figure 7. Effect of 10 µmol/L blebbistatin on the response of beat rate to stretch and release.

A: Normalized beat rate in one example preparation upon stretch (left) and release (right) under control conditions (top) and after the addition of blebbistatin (bottom); 5% uniaxial strain in the *x* direction. Same analysis as in Figure 5. B: Comparison of the normalized (fold) change in beat rate upon stretch and release under control conditions (labels "C") vs. with blebbistatin (labels "B"), for the 3 different target strains. *: $p<0.05$, paired Student's t-test. n=8 monolayer preparations obtained from 7 litters, except for the 2% biaxial strain protocol: n=7.

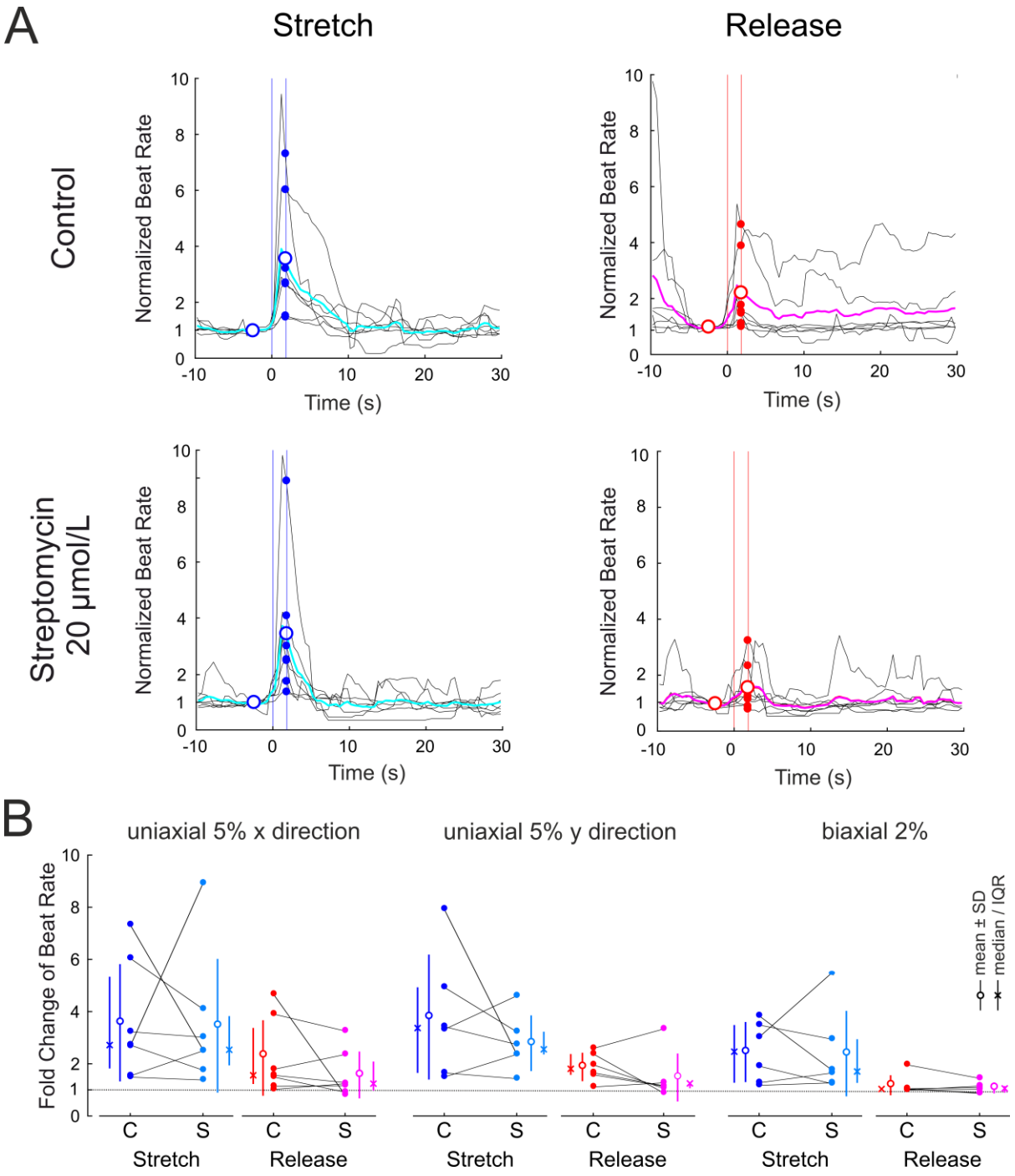

Figure 8. Effect 20 µmol/L streptomycin on the response of beat rate to stretch and release.

A: Normalized beat rate in one example preparation upon stretch (left) and release (right) under control conditions (top) and after the addition of streptomycin (bottom); 5% uniaxial strain in the *x* direction. Same analysis as in Figures 5 and 7. B: Comparison of the normalized (fold) change in beat rate upon stretch and release under control conditions (labels "C") vs. with streptomycin (labels "S"), for the 3 different strain protocols. n=6-7 monolayer preparations obtained from 5 litters. $p>0.05$ for all comparisons (paired Student's t-test).